Nonlinear force-free modeling of the solar coronal magnetic field

T. Wiegelmann[1]

[1]   The coronal magnetic field is an important quantity because the magnetic field dominates the structure of the solar corona. Unfortunately, direct measurements of coronal magnetic fields are usually not available. The photospheric magnetic field is measured routinely with vector magnetographs. These photospheric measurements are extrapolated into the solar corona. The extrapolated coronal magnetic field depends on assumptions regarding the coronal plasma, for example, force-freeness. Force-free means that all nonmagnetic forces like pressure gradients and gravity are neglected. This approach is well justified in the solar corona owing to the low plasma beta. One has to take care, however, about ambiguities, noise and nonmagnetic forces in the photosphere, where the magnetic field vector is measured. Here we review different numerical methods for a nonlinear force-free coronal magnetic field extrapolation: Grad-Rubin codes, upward integration method, MHD relaxation, optimization, and the boundary element approach. We briefly discuss the main features of the different methods and concentrate mainly on recently developed new codes.

1.   Introduction

1.1.   How to Obtain the Coronal Magnetic Field?

[2]   Information regarding the coronal magnetic field is important for space weather application like the onset of flares and coronal mass ejections (CMEs). Unfortunately, we usually cannot measure the coronal magnetic field directly, although recently some progress has been made [see, e.g., *Judge*, 1998; *Solanki et al.*, 2003; *Lin et al.*, 2004]. Because of the optically thin coronal plasma, direct measurements of the coronal magnetic field have a line-of-sight integrated character and to derive the accurate 3D structure of the coronal magnetic field a vector tomographic inversion is required. Corresponding feasibility studies based on coronal Zeeman and Hanle effect measurements have recently been done by *Kramar et al.* [2006] and *Kramar and Inhester* [2006]. These direct measurements are only available for a few individual cases and usually one has to extrapolate the coronal magnetic field from photospheric magnetic measurements. To do so, one has to make assumptions regarding the coronal plasma. It is helpful that the low solar corona is strongly dominated by the coronal magnetic field and the magnetic pressure is orders of magnitude higher than the plasma pressure. The quotient of plasma pressure p and magnetic pressure, $B^2/(2 \mu_0)$ is small compared to unity ($\beta = 2 \mu_0 p/B^2 \ll 1$). In lowest-order

nonmagnetic forces like pressure gradient and gravity can be neglected which leads to the force-free assumption. Force-free fields are characterized by the equations

$$\mathbf{j} \times \mathbf{B} = 0, \tag{1}$$

$$\nabla \times \mathbf{B} = \mu_0 \mathbf{j}, \tag{2}$$

$$\nabla \cdot \mathbf{B} = 0, \tag{3}$$

where $\mathbf{B}$ is the magnetic field, $\mathbf{j}$ the electric current density and μ_0 the permeability of vacuum. Equation (1) implies that for force-free fields the current density and the magnetic field are parallel, i.e.,

$$\mu_0 \mathbf{j} = \alpha \mathbf{B}, \tag{4}$$

or by replacing $\mathbf{j}$ with equation (2),

$$\nabla \times \mathbf{B} = \alpha \mathbf{B}, \tag{5}$$

where α is called the force-free function. To get some insights in the structure of the space-dependent function α, we take the divergence of equation (4) and make use of equations (2) and (3),

$$\mathbf{B} \cdot \nabla \alpha = 0, \tag{6}$$

which tells us that the force-free function α is constant on every field line, but will usually change from one field line

---

[1]Max-Planck-Institut für Sonnensystemforschung, Katlenburg-Lindau, Germany.

to another. This generic case is called nonlinear force-free approach.

[3] Popular simplifications are $\alpha = 0$ (current free potential fields [see, e.g., *Schmidt*, 1964; *Semel*, 1967; *Schatten et al.*, 1969; *Sakurai*, 1982]) and α = constant (linear force-free approach [see, e.g., *Nakagawa and Raadu*, 1972; *Chiu and Hilton*, 1977; *Seehafer*, 1978; *Alissandrakis*, 1981; *Seehafer*, 1982; *Semel*, 1988]). These simplified models have been in particular popular owing to their relative mathematical simplicity and because only line-of-sight photospheric magnetic field measurements are required. Linear force-free fields still contain one free global parameter α, which can be derived by comparing coronal images with projections of magnetic field lines [e.g., *Carcedo et al.*, 2003]. It is also possible to derive an averaged value of α from transverse photospheric magnetic field measurements [e.g., *Pevtsov et al.*, 1994; *Wheatland*, 1999; *Leka and Skumanich*, 1999]. Despite the popularity and frequent use of these simplified models in the past, there are several limitations in these models (see below) which ask for considering the more sophisticated nonlinear force-free approach.

[4] Our aim is to review recent developments of the extrapolation of nonlinear force-free fields (NLFFF). For earlier reviews on force-free fields we refer to *Sakurai* [1989], *Aly* [1989], *Amari et al.* [1997], *McClymont et al.* [1997], and chapter 5 of *Aschwanden* [2005]. Here we will concentrate mainly on new developments which took place after these earlier reviews. Our main emphasis is to study methods which extrapolate the coronal magnetic field from photospheric vector magnetograms. Several vector magnetographs are currently operating or planed for the nearest future, for example, ground based: the solar flare telescope/NAOJ [*Sakurai et al.*, 1995], the imaging vector magnetograph/MEES Observatory [*Mickey et al.*, 1996], Big Bear Solar Observatory, Infrared Polarimeter VTT, SOLIS/NSO [*Henney et al.*, 2006] and space born: Hinode/SOT [*Shimizu*, 2004], SDO/HMI [*Borrero et al.*, 2006]. Measurements from these vector magnetograms will provide us eventually with the magnetic field vector on the photosphere, say B_{z0} for the normal and B_{x0} and B_{y0} for the transverse field. Deriving these quantities from the measurements is an involved physical process, which includes measurements based on the Zeeman and Hanle effect, the inversion of Stokes profiles [e.g., *LaBonte et al.*, 1999] and removing the 180 ambiguity [e.g., *Metcalf*, 1994; *Metcalf et al.*, 2006] of the horizontal magnetic field component. Special care has to be taken for vector magnetograph measurements which are not close to the solar disk, when the line-of-sight and normal magnetic field component are far apart [e.g., *Gary and Hagyard*, 1990]. For the purpose of this paper we do not address the observational methods and recent developments and problems related to deriving the photospheric magnetic field vector. We rather will concentrate on how to use the photospheric B_{x0}, B_{y0} and B_{z0} to derive the coronal magnetic field.

[5] The transverse photospheric magnetic field (B_{x0}, B_{y0}) can be used to approximate the normal electric current distribution by

$$\mu_0 j_{z0} = \frac{\partial B_{y0}}{\partial x} - \frac{\partial B_{x0}}{\partial y}, \tag{7}$$

and from this one gets the distribution of α on the photosphere by

$$\alpha(x,y) = \mu_0 \frac{j_{z0}}{B_{z0}}. \tag{8}$$

[6] By using equation (8) one has to keep in mind that rather large uncertainties in the transverse field component and numerical derivations used in (7) can cumulate in significant errors for the current density. The problem becomes even more severe by using (8) to compute α in regions with a low normal magnetic field strength B_{z0}. Special care has to be taken at photospheric polarity inversion lines, i.e., lines along which $B_{z0} = 0$ [see, e.g., *Cuperman et al.*, 1991]. The nonlinear force-free coronal magnetic field extrapolation is a boundary value problem. As we will see later some of the NLFFF codes make use of (8) to specify the boundary conditions while other methods use the photospheric magnetic field vector more directly to extrapolate the field into the corona.

[7] Pure mathematical investigations of the nonlinear force-free equations [see, e.g., *Aly*, 1984; *Boulmezaoud and Amari*, 2000; *Aly*, 2005] and modeling approaches not based on vector magnetograms are important and occasionally mentioned in this paper. A detailed review of these topics is well outside the scope of this paper, however. Some of the model approaches not based on vector magnetograms are occasionally used to test the nonlinear force-free extrapolation codes described here.

1.2. Why Do We Need Nonlinear Force-Free Fields?

[8] 1. A comparison of global potential magnetic field models with TRACE images by *Schrijver et al.* [2005] revealed that significant nonpotentially occurs regularly in active regions, in particular when new flux has emerged in or close to the regions.

[9] 2. Usually α changes in space, even inside one active region. This can be seen, if we try to fit for the optimal linear force-free parameter α by comparing field lines with coronal plasma structures. An example is given by *Wiegelmann and Neukirch* [2002] where stereoscopic reconstructed loops by *Aschwanden et al.* [1999] have been compared with a linear force-free field model. The optimal value of α changes even sign within the investigated active regions, which is a contradiction to the α = constant linear force-free approach (see Figure 1).

[10] 3. Photospheric α distributions derived from vector magnetic field measurements by equation (8) show as well that α usually changes within an active region [see, e.g., *Régnier et al.*, 2002].

[11] 4. Potential and linear force-free fields are too simple to estimate the free magnetic energy and magnetic topology accurately. The magnetic energy of linear force-free fields is unbounded in a halfspace [*Seehafer*, 1978] which makes this approach unsuitable for energy approximations of the coronal magnetic field. Potential fields have a minimum energy for an observed line-of-sight photospheric magnetic field. An estimate of the excess of energy a configuration has above that of a potential field is an important quantity which might help to understand the onset of flares and coronal mass ejections.
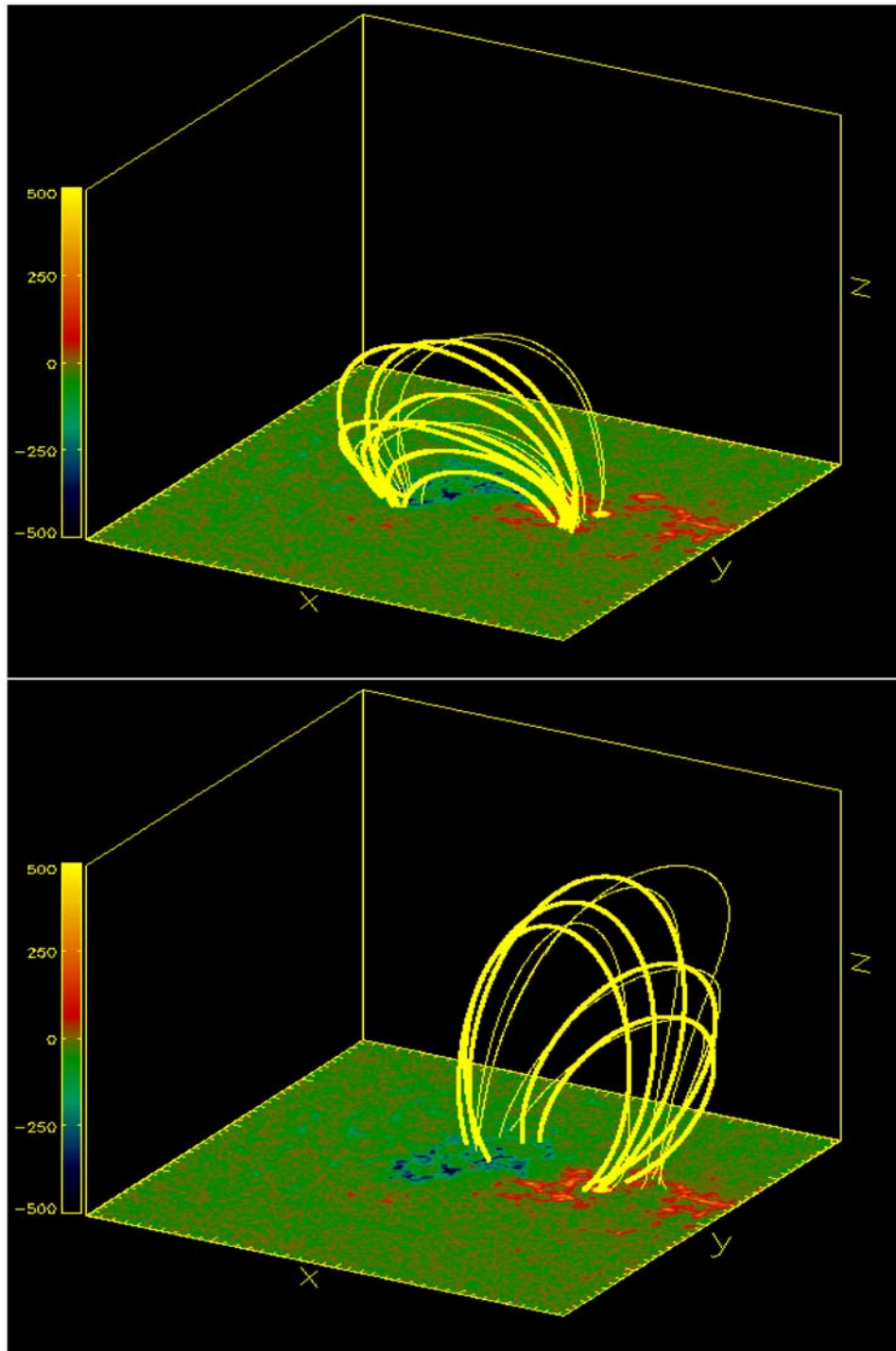
Figure 1. Linear force–free field model for NOAA 7986 with the best fit for α. (top) A group of loops with $\alpha = 2.5$ and (bottom) another group of loops with $\alpha = -2.0$. The different optimal values of the linear force-free parameter within one active region are a contradiction to the linear assumption (α constant) and tell us that a consistent modeling of this active regions requires nonlinear force-free approach. (This figure was originally published as *Wiegelmann and Neukirch*'s [2002] Figure 7). Used with permission of Springer.).

[12] 5. A direct comparison of measured fields in a newly developed active region by *Solanki et al.* [2003] with extrapolations from the photosphere with a potential, linear and nonlinear force-free model by *Wiegelmann et al.* [2005b] showed that nonlinear fields are more accurate than simpler models. Figure 2 shows some selected magnetic field lines for the original measured field and extrapolations from the photosphere with the help of a potential, linear and nonlinear force-free model.
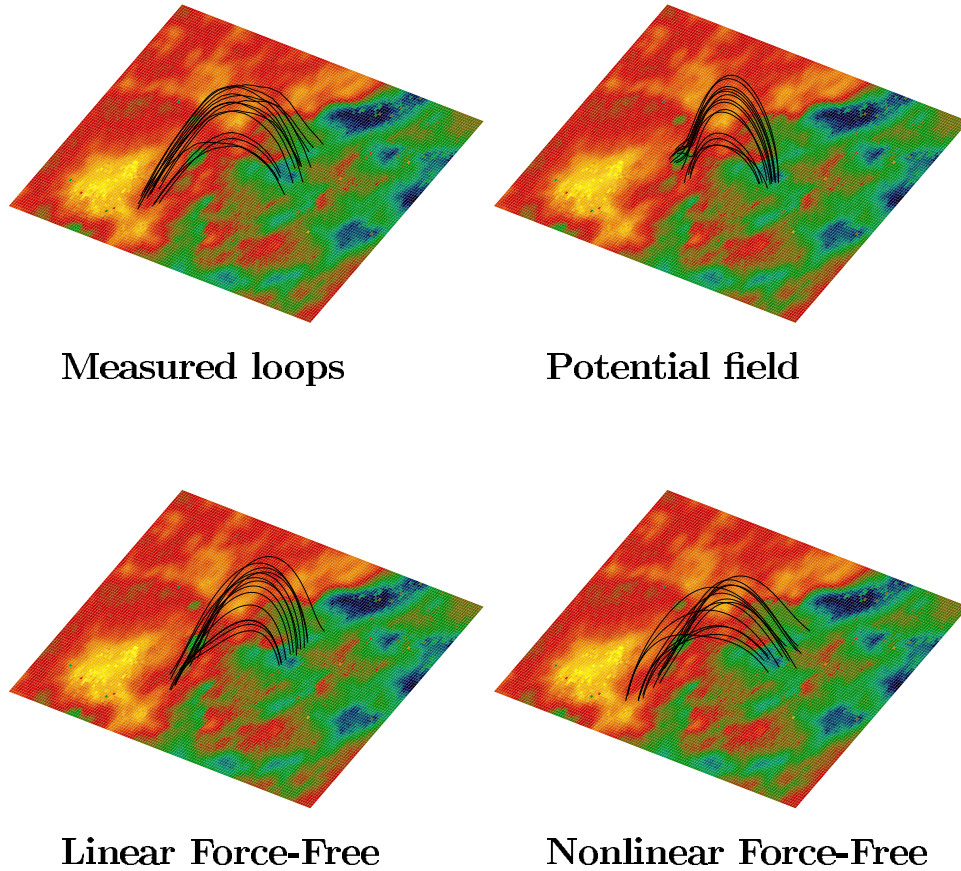
Figure 2. Magnetic field structure of the newly developed active region NOAA 9451. Direct measurements of the field have been compared with potential, linear, and nonlinear force-free models. Best agreement has been found for the nonlinear model. (This figure was originally published as part of *Wiegelmann et al.*'s [2005b] Figure 1. Used with permission of *Astronomy and Astrophysics*).

[13] These points tell us that nonlinear force-free modeling is required for an accurate reconstruction of the coronal magnetic field. Simpler models have been used frequently in the past. Global potential fields provide some information of the coronal magnetic field structure already, for example, the location of coronal holes. The generic case of force-free coronal magnetic field models are nonlinear force-free fields, however. Under generic we understand that α can (and usually will) change in space, but this approach also includes the special cases α = constant and α = 0. Some active regions just happen to be more potential (or linear force-free) and if this is the case they can be described with simpler models. Linear force-free models might provide a rough estimate of the true 3D magnetic field structure if the nonlinearity is weak. The use of simpler models was often justified owing to limited observational data, in particular if only the line-of-sight photospheric magnetic field has been measured.

[14] While the assumption of nonlinear force-free fields is well accepted for the coronal magnetic fields in active regions, this is not true for the photosphere. The photospheric plasma is a finite β plasma and nonmagnetic forces like pressure gradient and gravity cannot be neglected here. As a result electric currents have a component perpendicular to the magnetic field, which contradicts the force-free

assumption. We will discuss later how these difficulties can be overcome.

2. Nonlinear Force-Free Codes

[15] Different methods have been proposed to extrapolate nonlinear force-free fields from photospheric vector magnetic field measurements. (1) The Grad-Rubin method was proposed for fusion plasmas by *Grad and Rubin* [1958] and first applied to coronal magnetic fields by *Sakurai* [1981]. (2) The upward integration method was proposed by *Nakagawa* [1974] and encoded by *Wu et al.* [1985]. (3) The MHD relaxation method was proposed for general MHD equilibria by *Chodura and Schlueter* [1981] and applied to force-free coronal magnetic fields by *Mikic and McClymont* [1994]. (4) The optimization approach was developed by *Wheatland et al.* [2000]. (5) The boundary element (or Greens function like) method was developed by *Yan and Sakurai* [2000].

2.1. Grad-Rubin Method

[16] The Grad-Rubin method reformulates the nonlinear force-free equations in such a way, that one has to solve a well posed boundary value problem. This makes this approach also interesting for a mathematical investigation of the structure of the nonlinear force-free equations. *Bineau*

[1972] demonstrated that the used boundary conditions (vertical magnetic field on the photosphere and α distribution at one polarity) ensure, at least for small values of α and weak nonlinearities the existence of a unique nonlinear force-free solution. A detailed analysis of the mathematical problem of existence and uniqueness of nonlinear force-free fields is outside the scope of this review and is given, for example, by *Amari et al.* [1997, 2006].

[17] The method first computes a potential field, which can be obtained from the observed line-of-sight photospheric magnetic field (say B_z in Cartesian geometry) by different methods, for example, a Greens function method as described by *Aly* [1989]. It is also popular to use linear force-free solvers, for example, as implemented by *Seehafer* [1978] and *Alissandrakis* [1981] with the linear force-free parameter $\alpha = 0$ to compute the initial potential field. The transverse component of the measured magnetic field is then used to compute the distribution of α on the photosphere by equation (8). While α is described this way on the entire photosphere, for both polarities, a well posed boundary value problem requires that the α distribution becomes only described for one polarity. The basic idea is to iteratively calculate α for a given **B** field from (6), then calculate the current via (4) and finally update **B** from the Biot-Savart problem (5). These processes are repeated until the full current as prescribed by the α distribution has been injected into the magnetic field and the updated magnetic field configuration becomes stationary in the sense that eventually the recalculation of the magnetic field with Amperes law does not change the configuration anymore. To our knowledge the Grad-Rubin approach has been first implemented by *Sakurai* [1981]. Here α has been prescribed on several nodal points along a number of magnetic field lines of the initial potential field. The method used a finite-element-like discretization of current tubes associated with magnetic field lines. Each current tube was divided into elementary current tubes of cylindrical shape. The magnetic field is updated with Ampere's law using a superposition of the elementary current tubes. The method was limited by the number of current-carrying field lines, nodal points and the corresponding number of nonlinear equations (N^9) to solve with the available computer resources more than a quarter century ago.

[18] Computer resources have increased rapidly since the first NLFFF implementation by *Sakurai* [1981] and about a decade ago the Grad-Rubin method has been implemented on a finite difference grid by *Amari et al.* [1997, 1999]. This approach decomposes equations (1)–(3) into a hyperbolic part for evolving α along the magnetic field lines and an elliptic one to iterate the updated magnetic field from Amperes law. For every iteration step k one has to solve iteratively for

$$\mathbf{B}^{(k)} \cdot \nabla \alpha^{(k)} = 0 \tag{9}$$

$$\alpha^{(k)} \mid_{S\pm} = \alpha_{0\pm}, \tag{10}$$

which evolves α in the volume and

$$\nabla \times \mathbf{B}^{(k+1)} = \alpha^{(k)} \mathbf{B}^{(k)}, \tag{11}$$

$$\nabla \cdot \mathbf{B}^{(k+1)} = 0, \tag{12}$$

$$B_z^{(k+1)} \mid_{S\pm} = B_{z0}, \tag{13}$$

$$\lim_{|r| \to \infty} \mid \mathbf{B}^{(k+1)} \mid = 0, \tag{14}$$

where $\alpha_{0\pm}$ corresponds to the photospheric distribution of α for either on the positive or the negative polarity. The Grad-Rubin method as described by *Amari et al.* [1997, 1999] has been applied to investigate particular active regions by *Bleybel et al.* [2002] and a comparison of the extrapolated field with 2D projections of plasma structures as seen in Hα, EUV and X ray has been done by *Régnier et al.* [2002] and *Régnier and Amari* [2004]. The code has also been used to investigate mutual and self helicity in active regions by *Régnier et al.* [2005] and to flaring active regions by *Régnier and Canfield* [2006].

[19] A similar approach as done by *Sakurai* [1981] has been implemented by *Wheatland* [2004]. The implemented method computes the magnetic field directly on the numerical grid from Ampere's law. This is somewhat simpler and faster as Sakurai's approach which required solving a large system of nonlinear equations for this aim. The implementation by *Wheatland* [2004] has, in particular, been developed with the aim of parallelization. The parallelization approach seems to be effective owing to a limited number of interprocess communications. This is possible because as the result of the linearity of Ampere's law the contributions of the different current carrying field lines are basically independent from each other. In the original paper Wheatland reported problems for large currents on the field lines. These problems have been related to an error in current representation of the code and the corrected code worked significantly better [see also *Schrijver et al.*, 2006]. The method has been further developed by *Wheatland* [2006]. This newest Wheatland-implementation scales with the number of grid points N^4 for a N^3 volume, rather than N^6 for the earlier [*Wheatland*, 2004] implementation. The main new development is a faster implementation of the current-field iteration. To do so the magnetic field has been separated into a current-free and a current carrying part at each iteration step. Both parts are solved using a discrete Fast Fourier Transformation, which imposes the required boundary conditions implicitly. The code has been parallelized on shared memory distributions with OpenMP.

[20] *Amari et al.* [2006] developed two new versions of their Grad-Rubin code. The first version is a finite difference method and the code was called 'XTRAPOL.' This code prescribe the coronal magnetic field with the help of a vector potential **A**. The code has obviously it's heritage from the earlier implementation of *Amari et al.* [1999], but with several remarkable differences:

[21] 1. The code includes a divergence cleaning routine, which takes care about $\nabla \cdot \mathbf{A} = 0$. The condition $\nabla \cdot \mathbf{A} = 0$ is fulfilled with high accuracy in the new code 10^{-9} compared to 10^{-2} in the earlier implementation.

[22] 2. The lateral and top boundaries are more flexible compared to the earlier implementation and allow a finite B_n

and non zero α values for one polarity on all boundaries. This treats the whole boundary (all six faces) as a whole.

[23] 3. The slow current input as reported for the earlier implementation, which lead to a two level iteration, has been replaced. Now the whole current is injected at once and only the inner iteration loop of the earlier code remained in the new version.

[24] 4. The computation of the α characteristics has been improved with an adaptive Adams-Bashforth integration scheme (see *Press* [2002] for details).

[25] 5. The fixed number of iteration loops have been replaced by a quantitative convergence criterium.

[26] In the same paper [*Amari et al.*, 2006] introduced another Grad-Rubin approach based on finite elements, which they called 'FEMQ'. Different from alternative implementation this code does not use a vector potential but iterates the coupled divergence and curl system, which is solved with the help of a finite element discretization. The method transforms the nonlinear force-free equations into a global linear algebraic system.

[27] *Inhester and Wiegelmann* [2006] implemented a Grad-Rubin code on a finite element grid with staggered field components [see *Yee*, 1966] which uses discrete Whitney forms [*Bossavit*, 1988]. Whitney forms allow to transform standard vector analysis (as the differential operators gradient, curl and divergence) consistently into the discrete space used for numerical computations. Whitney forms contain four types of finite elements (form 0–3). They can be considered as a discrete approximation of differential forms. The finite element base may consist of polynomials of any order. In its simplest form, the 0-forms have as parameters the function values at the vertices of the cells and are linearly interpolated within each cell. The 1-forms are a discrete representation of a vector field defined on the cell edges. The 2-forms are defined as the field component normal to the surfaces of the cells. The 3-forms are finite volume elements for a scalar function approximation, which represents the average of a scalar over the entire cell. The 4-forms are related to each other by GRAD (0 to 1 form), CURL (1 to 2 form) and DIV (2 to 3 form). As for continuous differential forms, double differentiation (CURL of GRAD, DIV of CURL) give exactly zero, independent of the numerical precision. A dual grid, shifted by half a grid size in each axis, was introduced in order to allow for Laplacians. Whitney forms on the dual grid are related to forms on the primary grid in a consistent way.

[28] The Grad-Rubin implementation uses a vector potential representation of the magnetic field, where the vector potential is updated with a Poisson equation in each iteration step. The Poisson equation is effectively solved with the help of a multigrid solver. The main computing time is spend to distribute α along the field lines with (6). This seems to be a general property of Grad-Rubin implementations. One can estimate the scaling of (6) by $\propto N^4$, where the number of field lines to compute is $\propto N^3$ and the length of a field line $\propto N$. The Biot-Savart step (5) solved with FFT or multigrid methods scales only with $\propto N \log N$. Empirical tests show that the number of iteration steps until a stationary state is reached does not depend on the number of grid points N for Grad-Rubin solvers. We have explained before, that the Grad-Rubin implementation requires the prescription of α only for one polarity to have a well posed

mathematical problem. The *Inhester and Wiegelmann* [2006] implementation allows these choice of boundary conditions as a special case. In general one does not need to make the distinction between $(\partial V)^+$ and $(\partial V)^-$ in the new implementation. A well posed mathematical problem is still ensured, however, in the following way. Each boundary value of α is attached with a weight. The final version of α on each field line is then determined by a weighted average of the α values on both endpoints of a field lines. By this way the influence of uncertain boundary values, for example, on the side walls and imprecise photospheric measurements can be suppressed.

2.2. Upward Integration Method

[29] The basic equations for the upward integration method (or progressive extension method) have been published already by *Nakagawa* [1974] and a corresponding code has been developed by *Wu et al.* [1985, 1990a]. The upward integration method is a straight forward approach to use the nonlinear force-free equations directly to extrapolate the photospheric magnetic field into the corona. To do so one reformulates the force-free equations (1)–(3) in order to extrapolate the measured photospheric magnetic field vector into the solar corona.

[30] As a first step the magnetic field vector on the lower boundary $\mathbf{B}_0(x,y,0)$ is used to compute the z component of the electric current $\mu_0 j_{z0}$ with equation (7) and the photospheric α distribution (say α_0) by equation (8). With the help of equation (4) we calculate the x and y component of the current density

$$\mu_0 j_{x0} = \alpha_0 B_{x0} \tag{15}$$

$$\mu_0 j_{y0} = \alpha_0 B_{y0}. \tag{16}$$

[31] We now use equation (3) and the x and y component of equation (2) to obtain expressions for the z derivatives of all three magnetic field components in the form

$$\frac{\partial B_{x0}}{\partial z} = \mu_0 j_{y0} + \frac{\partial B_{z0}}{\partial x}, \tag{17}$$

$$\frac{\partial B_{y0}}{\partial z} = \frac{\partial B_{z0}}{\partial y} - \mu_0 j_{x0}, \tag{18}$$

$$\frac{\partial B_{z0}}{\partial z} = -\frac{\partial B_{x0}}{\partial x} - \frac{\partial B_{y0}}{\partial y}. \tag{19}$$

The idea is to integrate this set of equations numerically upward in z by repeating the previous steps at each height. As a result we get in principle the 3D magnetic field vector in the corona. While this approach is straight forward, easy to implement and computational fast (no iteration is required), a serious drawback is that it is unstable. Several authors [e.g., *Cuperman et al.*, 1990; *Amari et al.*, 1997] pointed out that the formulation of the force-free equations in this way is unstable because it is based on an ill-posed mathematical problem. In particular one finds that expo-

nential growth of the magnetic field with increasing height is a typical behavior. What makes this boundary value problem ill-posed is that the solution does not depend continuously on the boundary data. Small changes or inaccuracies in the measured boundary data lead to a divergent extrapolated field (see *Low and Lou* [1990] for a more detailed discussion). As pointed out by Low and Lou meaningful boundary conditions are required also on the outer boundaries of the computational domain. It is also possible to prescribe open boundaries in the sense that the magnetic field vanishes at infinity. This causes an additional problem for the upward integration method, because the method transports information only from the photosphere upward and does not incorporate boundary information on other boundaries or at infinity. Attempts have been made to regularize the method [e.g., *Cuperman et al.*, 1991; *Demoulin and Priest*, 1992], but cannot be considered as fully successful.

[32] *Wu et al.* [1990b] compared the Grad-Rubin method in the implementation of *Sakurai* [1981] with the upward integration method in the implementation of *Wu et al.* [1990a]. (The authors used a somewhat different nomenclature: The upward integration method was called 'progressive extension method' and the Grad-Rubin method 'iterative method'. That time the term 'iterative method' was reasonable because Grad-Rubin was the only iterative approach available, but now, 17 years later, several other iterative methods are available to compute nonlinear force-free fields.) The comparison showed qualitatively similar results for extrapolations from an observed magnetogram, but quantitatively differences. The NLFFF computations have been very similar to potential field extrapolations, however, too. One reason for this behavior was, that the method of *Sakurai* [1981] is limited to small values of α and a 'by eye' comparison shows that the corresponding NLFFF field is very close to a potential field configuration. The field computed with the upward integration method deteriorated if the height of the extrapolation exceeded a typical horizontal scale length.

[33] The upward integration method has been recently reexamined by *Song et al.* [2006] who developed a new formulation of this approach. The new implementation uses smooth continuous functions and the equations are solved in asymptotic manner iteratively. The original upward integration equations are reformulated into a set of ordinary differential equations and uniqueness of the solution seems to be guaranteed at least locally. While *Demoulin and Priest* [1992] stated that 'no further improvement has been obtained with other types of smoothing functions' *Song et al.* [2006] point out that the transformation of the original partial differential equations into ordinary ones eliminates the growing modes in the upward integration method, which have been reported before by *Wu et al.* [1990a] and subsequent papers. The problem that all three components of the photospheric magnetic field and the photospheric α distribution has to be prescribed in a consistent way remains in principle, but some compatibility conditions to compute a slowly varying α have been provided by *Song et al.* [2006]. These compatibility conditions are slightly different for real photospheric observations and tests with smooth boundaries extracted from semianalytic equilibria. For the latter kind of problems the new formulation provided reasonable results

with the standard test equilibrium found by *Low and Lou* [1990]. The method seems to be also reasonably fast. Of course, further tests with more sophisticated equilibria and real data are necessary to evaluate this approach in more detail.

2.3. MHD Relaxation

[34] MHD relaxation codes [e.g., *Chodura and Schlueter*, 1981] can be applied to solve nonlinear force-free fields as well. The idea is to start with a suitable magnetic field which is not in equilibrium and to relax it into a force-free state. This is done by using the MHD equations in the following form:

$$v\mathbf{v} = (\nabla \times \mathbf{B}) \times \mathbf{B}, \qquad (20)$$

$$\mathbf{E} + \mathbf{v} \times \mathbf{B} = 0, \qquad (21)$$

$$\frac{\partial \mathbf{B}}{\partial t} = -\nabla \times \mathbf{E}, \qquad (22)$$

$$\nabla \cdot \mathbf{B} = 0, \qquad (23)$$

where v is a viscosity and $\mathbf{E}$ the electric field. As the MHD relaxation aims for a quasiphysical temporal evolution of the magnetic field from a nonequilibrium toward a (nonlinear force-free) equilibrium this method is also called 'evolutionary method' or 'magneto-frictional method'. The basic idea is that the velocity field in the equation of motion (21) is reduced during the relaxation process. Ideal Ohm's law (22) ensures that the magnetic connectivity remains unchanged during the relaxation. The artificial viscosity v plays the role of a relaxation coefficient which can be chosen in such way that it accelerates the approach to the equilibrium state. A typical choice is

$$v = \frac{1}{\mu} \mid \mathbf{B} \mid^2, \qquad (24)$$

with μ = constant. Combining equations (20), (21), (22) and (24) we get an equation for the evolution of the magnetic field during the relaxation process,

$$\frac{\partial \mathbf{B}}{\partial t} = \mu \mathbf{F}_{MHD}, \qquad (25)$$

with

$$\mathbf{F}_{MHD} = \nabla \times \left(\frac{[(\nabla \times \mathbf{B}) \times \mathbf{B}] \times \mathbf{B}}{B^2} \right). \qquad (26)$$

This equation is then solved numerically starting with a given initial condition for $\mathbf{B}$, usually a potential field. Equation (25) ensures that equation (23) is satisfied during the relaxation if the initial magnetic field satisfies it. (As we will see below the 'optimization' approach leads to a similar iteration equations for the magnetic field, but a different artificial driving force $\mathbf{F}$.) The difficulty with this method is that it cannot be guaranteed that for given boundary

conditions and initial magnetic field (i.e., given connectivity), a smooth force-free equilibrium exists to which the system can relax. If such a smooth equilibrium does not exist the formation of current sheets is to be expected which will lead to numerical difficulties. Therefore care has to be taken when choosing an initial magnetic field.

[35] *Yang et al.* [1986] developed a magneto frictional method which represent the magnetic field with the help of Euler (or Clebsch) potentials.

$$\mathbf{B} = \nabla g \times \nabla h, \qquad (27)$$

where the potentials g and h are scalar functions. The general method has been developed for three dimensional fields and iterative equations for $g(x, y, z)$ and $h(x, y, z)$ have been derived. The Clebsch representation automatically ensures $\nabla \cdot \mathbf{B} = 0$. The method has been explicitly tested in the paper by [*Yang et al.*, 1986] with the help of an equilibrium with one invariant coordinate. In principle it should be possible to use this representation for the extrapolation of nonlinear force-free fields, but we are not aware of a corresponding implementation. On the basis of the discussion by *Yang et al.* [1986] a difficulty seems to be that one needs to specify boundary conditions for the potentials, rather than for the magnetic fields. It seems in particular to be difficult to find boundaries conditions for potentials which correspond to the transverse component of the photospheric magnetic field vector. One problem is that boundary conditions for g and h prescribe the connectivity. Every field line can be labeled by its (g,h) values. Hence boundary values for g and h establish foot point relations although the field is not known yet.

[36] The MHD relaxation (or evolutionary) method has been implemented by *Mikic and McClymont* [1994] and *McClymont et al.* [1997] on the basis of the time-dependent MHD code by *Mikic et al.* [1988]. The code uses a nonuniform mesh and the region of interested is embedded in a large computational domain to reduce the influence of the lateral boundaries. The method has been applied to extrapolate the magnetic field above an active region by *Jiao et al.* [1997]. The computations have been carried out with a resolution of the order of 100^3 points. A supercomputer was required for these computations that time (10 years ago), but because of the rapid increase of computer speed and memory within the last decade this restriction is very probably not valid anymore.

[37] *Roumeliotis* [1996] developed the so-called stress and relax method. In this approach the initial potential field becomes disturbed by the observed transverse field component on the photosphere. The boundary conditions are replaced in subsequently in several small steps and always relaxed with a similar MHD relaxation scheme as described above toward a force-free equilibrium. The code by *Roumeliotis* [1996] has implemented a function $w(x,y)$ which allows to give a lower weight to regions where the transverse photospheric field has been measured with lower accuracy. Additional to the iterative equations as discussed above, the method includes a resistivity η (or diffusivity) by adding a term $\eta \mathbf{j}$ on the right hand site of Ohms law (21). This relaxes somewhat the topological constrains of ideal MHD relaxation, because a finite resistivity allows a kind of artificial reconnection and corresponding changes of the initial potential field topology. The method has been tested with a force-free equilibrium found by *Klimchuk and Sturrock* [1992] and applied to an active region measured with the MSFC vector-magnetograph.

[38] The stress and relax method has been revisited by *Valori et al.* [2005]. Different from the earlier implementation by *Roumeliotis* [1996] the new implementation uses directly the magnetic field, rather than the vector potential in order to keep errors from taking numerical deviations from noisy magnetograms minimal. The solenoidal condition is controlled by a diffusive approach by *Dedner et al.* [2002] which removes effectively a numerically created finite divergence of the relaxed magnetic field. The new implementation uses a single stress step, rather than the multiple small stress used by *Roumeliotis* [1996] to speed up the computation. The single step stress and relax method is connected with a suitable control of artificial plasma flows by the Courant criterium. The authors reported that a multistep and single-step implementation do not reveal significant differences. The numerical implementation is based on the time-dependent full MHD code 'AMRVAC' by *Keppens et al.* [2003]. *Valori et al.* [2005] tested their nonlinear force-free implementation with a numerically constructed nonlinear force-free twisted loop computed by *Török and Kliem* [2003].

2.4. Optimization Approach

[39] The optimization approach has been developed by *Wheatland et al.* [2000]. The solution is found by minimizing the functional

$$L = \int_V [B^{-2} \mid (\nabla \times \mathbf{B}) \times \mathbf{B} \mid^2 + \mid \nabla \cdot \mathbf{B} \mid^2]d^3V. \qquad (28)$$

Obviously, L is bound from below by 0. This bound is attained if the magnetic field satisfies the force-free equations (1)−(3).

[40] By taking the functional derivatives with respect to some iteration parameter t we get

$$\Rightarrow \frac{1}{2}\frac{dL}{dt} = -\int_V \frac{\partial \mathbf{B}}{\partial t} \cdot \tilde{\mathbf{F}}d^3x - \int_S \frac{\partial \mathbf{B}}{\partial t} \cdot \tilde{\mathbf{G}}d^2x, \qquad (29)$$

with

$$\mathbf{F} = \nabla \times \left(\frac{[(\nabla \times \mathbf{B}) \times \mathbf{B}] \times \mathbf{B}}{B^2}\right) + \left\{-\nabla \times \left(\frac{((\nabla \cdot \mathbf{B})\mathbf{B}) \times \mathbf{B}}{B^2}\right)\right.$$
$$\left. - \Omega \times (\nabla \times \mathbf{B}) - \nabla(\Omega \cdot \mathbf{B}) + \Omega(\nabla \cdot \mathbf{B}) + \Omega^2\mathbf{B}\right\} \qquad (30)$$

$$\Omega = \mathbf{B}^{-2}[(\nabla \times \mathbf{B}) \times \mathbf{B} - (\nabla \cdot \mathbf{B})\mathbf{B}]. \qquad (31)$$

The surface term vanishes if the magnetic field vector is kept constant on the surface, for example, prescribed from photospheric measurements. In this case L decreases monotonically if the magnetic field is iterated by

$$\frac{\partial \mathbf{B}}{\partial t} = \mu\mathbf{F}. \qquad (32)$$

[41] Let us remark that $\mathbf{F}_{MHS}$ as defined in equation (26) and used for MHD relaxation is identical with the first term on the right-hand-side of equation (30), but equation (30) contains additional terms.

[42] For this method the vector field $\mathbf{B}$ is not necessarily solenoidal during the computation, but will be divergence-free if the optimal state with $L = 0$ is reached. A disadvantage of the method is that it cannot be guaranteed that this optimal state is indeed reached for a given initial field and boundary conditions. If this is not the case then the resulting $\mathbf{B}$ will either be not force-free or not solenoidal or both.

[43] McTiernan has implemented the optimization approach basically as described by *Wheatland et al.* [2000] in IDL (see *Schrijver et al.* [2006] for a brief description of the McTiernan implementation). This code allows the use of a nonuniform computational grid. In a code intercomparison by *Schrijver et al.* [2006] the IDL optimization code by McTiernan was about a factor of 50 slower compared to an implementation in parallelized C by *Wiegelmann* [2004]. To our knowledge McTiernan has translated his IDL code into FORTRAN in the meantime for faster computation (J. M. McTiernan, personal communication on the NLFFF workshop Palo Alto, June 2006 [see also *Metcalf et al.*, 2007]).

[44] Several tests have been performed with the optimization approach of *Wiegelmann and Neukirch* [2003]. It has been investigated how the unknown lateral and top boundary influence the solution. The original optimization approach by *Wheatland et al.* [2000] has been extended toward more flexible boundary conditions, which allow $\frac{\partial B}{\partial t} \neq 0$ on the lateral and top boundaries. This has been made with the help of the surface integral term in (29) and led to an additional term $\frac{\partial B}{\partial t} = \mu\mathbf{G}$ on the boundaries. This approached improved the performance of the code for cases where only the bottom boundary was prescribed. No improvement was found for a slow multistep replacement of the boundary and this possibility has been abandoned in favor of a single step method. It has been also investigated how noise influences the optimization code and this study revealed that noise in the vector magnetograms leads to less accurate nonlinear force-free fields.

[45] *Wiegelmann* [2004] has reformulated the optimization principle by introducing weighting functions One defines the functional

$$L = \int_V [wB^{-2} \mid (\nabla \times \mathbf{B}) \times \mathbf{B} \mid^2 + w \mid \nabla \cdot \mathbf{B} \mid^2]d^3x, \quad (33)$$

where $w(x, y, z)$ is a weighting function. It is obvious that (for $w > 0$) the force-free equations (1−3) are fulfilled when L is equal zero. Minimization of the functional (34) lead to

$$\frac{\partial \mathbf{B}}{\partial t} = \mu\tilde{\mathbf{F}}, \quad (34)$$

$$\tilde{\mathbf{F}} = w\mathbf{F} + (\Omega_a \times \mathbf{B}) \times \nabla w + (\Omega_b \cdot \mathbf{B})\nabla w, \quad (35)$$

$$\Omega_a = B^{-2}[(\nabla \times \mathbf{B}) \times \mathbf{B}], \quad (36)$$

$$\Omega_b = B^{-2}[(\nabla \cdot \mathbf{B})\mathbf{B}], \quad (37)$$

with $\mathbf{F}$ as defined in (30). With $w(x, y, z) = 1$ this approach reduces to the *Wheatland et al.* [2000] method as described above. The weighting function is useful if only the bottom boundary data are known. In this case we a buffer boundary of several grid points toward the lateral and top boundary of the computational box is introduced. The weighting function is chosen constant in the inner, physical domain and drop to 0 with a cosine profile in the buffer boundary toward the lateral and top boundary of the computational box. In the work of *Schrijver et al.* [2006] some tests have been made with different weighting functions for the force-free and solenoidal part of the functional (34), but the best results have been obtained if both terms got the same weight. The computational implementation involves the following steps.

[46] 1. Compute start equilibrium (e.g., a potential field) in the computational box.

[47] 2. Replace the bottom boundary with the vector magnetogram.

[48] 3. Minimize the functional (33) with the help of equation (34). The continuous form of (34) guaranties a monotonically decreasing L. This is as well ensured in the discretized form if the iteration step dt is sufficiently small. The code checks if $L(t+dt) < L(t)$ after each time step. If the condition is not fulfilled, the iteration step is repeated with dt reduced by a factor of 2. After each successful iteration step we increase dt slowly by a factor of 1.01 to allow the time step to become as large as possible with respect to the stability condition.

[49] 4. The iteration stops if L becomes stationary. Stationarity is assumed if $\frac{\partial L}{\partial t}/L < 1.0 \ 10^{-4}$ for 100 consecutive iteration steps.

[50] The program has been tested with the semianalytic nonlinear force-free configuration of *Low and Lou* [1990] and *Titov and Démoulin* [1999] by *Wiegelmann et al.* [2006a]. The code has been applied to extrapolate the coronal magnetic field in active regions by *Wiegelmann et al.* [2005b, 2005a].

[51] A finite element optimization approach has been implemented by *Inhester and Wiegelmann* [2006] using the Whitney elements as for the Grad-Rubin code (which has been described above). The optimization method uses exactly the same staggered finite element grid as described above, which is different from the finite difference grids used in the earlier implementations by *Wheatland et al.* [2000], *Wiegelmann and Neukirch* [2003], and *Wiegelmann* [2004]. Another difference is that earlier implementations discretized the analytical derivative of the functional L (28), while the new code takes the numerical more consistent derivative of the discretized function L. All other implementations used a simple Landweber scheme for updating the magnetic field, which is replaced here by an unpreconditioned conjugate gradient iteration, which at every time step performs an exact line search to the minimum of L in the current search direction and additional selects an improve search direction instead of the gradient of the functional L. To do so the Hessian matrix of the functional L is computed during every iteration step. An effective computation of the Hessian matrix is possible, because the reformulated function $L(s)$ is a fourth-order polynomial in $\mathbf{B}$ and all five polynomial coefficients can be computed in one go. The code has been tested by *Low and Lou* [1990] and the

result of twisted loop computations of the Grad-Rubin implementation on the same grid.

[52] The optimization code in the implementation of *Wiegelmann* [2004] has recently been extended toward using a multiscale implementation. The main difference from the original code are [see also *Metcalf et al.*, 2007] as follows. (1) The method is not full multigrid, but computes the solution on different grids only once, for example, something like 50^3, 100^3, 200^3. (2) The main idea is to get a better (than potential field) start equilibrium on the full resolution box. (3) Solution of smaller grids are interpolated onto larger grids as initial state for the magnetic field in the computational domain of the next larger box. The multiscale implementation has been tested as part of a code-intercomparison test by *Metcalf et al.* [2007] with the help of solar-like reference model computed by *van Ballegooijen* [2004] and *van Ballegooijen et al.* [2007].

[53] The optimization approach has recently been implemented in spherical geometry by *Wiegelmann* [2007] and tested by *Low and Lou* [1990]. The original longitudinal symmetric Low and Lou solution has been shifted by 1/4 of a solar radius to test the code without any symmetry with respect to the Suns surface. The numerical implementation is very similar as the Cartesian implementation described by *Wiegelmann* [2004]. The spherical implementation converged fast for low-latitude regions, but the computing time increased significantly if polar regions have been included. It has been suggested to implement the code on a so called 'Yin and Yang' grid as developed by *Kageyama and Sato* [2004] to reduce the computing time. The 'Yin and Yang' grid is suitable for massive parallelization, which is necessary for full-sphere high-resolution NLFFF computations.

2.5. Boundary Element or Greens-Function-Like Method

[54] The boundary integral method has been developed by *Yan and Sakurai* [2000]. The method relates the measured boundary values with the nonlinear force-free field in the entire volume by

$$c_i\mathbf{B_i} = \oint_S \left(\bar{\mathbf{Y}}\frac{\partial \mathbf{B}}{\partial n} - \frac{\partial \bar{\mathbf{Y}}}{\partial n}\mathbf{B}_0 \right)d\mathbf{S}, \qquad (38)$$

where $c_i = 1$ for points in the volume and $c_i = 1/2$ for boundary points and $\mathbf{B}_0$ is the measured vector magnetic field on the photosphere. The auxiliary vector function is defined as

$$\bar{\mathbf{Y}} = \mathrm{diag}\left(\frac{\cos(\lambda_x r)}{4\pi r}, \frac{\cos(\lambda_y r)}{4\pi r}, \frac{\cos(\lambda_z r)}{4\pi r} \right), \qquad (39)$$

and the λ_i, $(i = x, y, z)$ are computed in the original approach by *Yan and Sakurai* [2000] with integrals over the whole volume, which define the λ_i implicitly,

$$\int_V Y_i[\lambda_i^2 B_i - \alpha^2 B_i - (\nabla\alpha \times \mathbf{B}_i)]dV = 0. \qquad (40)$$

This volume integration, which has to be carried out for every point in the volume is certainly very time consuming (a sixth-order process). The λ_i have the same dimension as

the magnetic field. The existence of the λ_i has been confirmed for the semianalytic field of *Low and Lou* [1990] by *Li et al.* [2004]. While the work of *Li et al.* [2004] showed that one can find the auxiliary function $\bar{\mathbf{Y}}$ for a given force-free field in 3D, the difficulty is that $\bar{\mathbf{Y}}$ is a priori unknown if only the photospheric magnetic field vector is given. *Yan and Sakurai* [2000] proposed an iterative scheme to compute the auxiliary functions and the nonlinear force-free magnetic field self-consistently. They use the approximate solution k on the right-hand side of equation (38) to compute a better solution $k + 1$ by

$$c_i\mathbf{B_i}^{(k+1)} = \oint_S \left(\bar{\mathbf{Y}}^{(\mathbf{k})}\frac{\partial \mathbf{B}^{(\mathbf{k})}}{\partial n} - \frac{\partial \bar{\mathbf{Y}}^{(\mathbf{k})}}{\partial n}\mathbf{B}_0 \right)d\mathbf{S}, \qquad (41)$$

where the initial guess for the magnetic field in the volume is $\mathbf{B} = 0$ and also the initial $\frac{\partial \bar{\mathbf{Y}}}{\partial n} = 0$. In principle it would be also possible to compute a potential field first and derive the auxiliary functions for this field as done by *Li et al.* [2004] and iterate subsequently for the nonlinear force-free fields and the associated auxiliary functions with equation (41). This possibility has not been tried out to our knowledge until now, however. The method iterates the magnetic field until $\mathbf{B}$ and $\frac{\partial \mathbf{B}}{\partial n}$ converge. In an inter code comparison by *Schrijver et al.* [2006] one iteration step of (41) took about 80 hours for this method and only this one step was carried out without further iteration. This seems, however, not to be sufficient to derive an accurate nonlinear force-free solution. The method has been applied for the comparison with soft X-ray loops observed with YOHKOH by *Wang et al.* [2000] and *Liu et al.* [2002] and to model a magnetic flux robe by *Yan et al.* [2001a, 2001b].

[55] In a new implementation of the boundary element method by *Yan and Li* [2006] the auxiliary functions are computed iteratively with the help of a simplex method. This avoids the numerical expensive computation of the volume integral (40). The boundary element method is still rather slow if a magnetic field has to be computed in an entire 3D domain. Different from other method, it allows, however, to evaluate the NLFFF field at every arbitrary point within the domain from the boundary data, without the requirement to compute the field in an entire domain. This is in particular useful if one is interested to compute the NLFFF field only along a given loop.

[56] *He and Wang* [2006] investigated the validity of the boundary integral representation for a spherical implementation. The method has been tested with the longitudinal invariant [*Low and Lou*, 1990] solution. The spherical implementation method of this method revealed reasonable results for smooth modestly nonlinear fields, but a poor convergence for complex magnetic field structures and large values of α.

3. How to Deal With Non-Force-Free Boundaries and Noise?

[57] Given arbitrary boundary conditions of the magnetic field vector on the photosphere, the solution to the force-free equations in 3D may not exist. Nonlinear force-free coronal magnetic field models assume, however, that the solution exists. It is certainly possible and necessary to

check after or during the computation if a solution has been found. In the following we will discuss what we can do if the measured photospheric data are incompatible with the assumption of a force-free coronal magnetic field.

3.1. Consistency Check of Vector Magnetograms

[58] We reexamine some necessary conditions with the photospheric field (or bottom boundary of a computational box). These conditions have to be fulfilled in order to be suitable boundary conditions for a nonlinear force-free coronal magnetic field extrapolation. An a priori assumption about the photospheric data is that the magnetic flux from the photosphere is sufficiently distant from the lateral boundaries of the observational domain and the net flux is in balance, i.e.,

$$\int_S B_z(x, y, 0) dx dy = 0. \tag{42}$$

Molodensky [1969, 1974], *Aly* [1989], and *Sakurai* [1989] used the viral theorem to define which conditions a vector magnetogram has to fulfill to be consistent with the assumption of a force-free field in the corona above the boundary. These conditions are as follows.

[59] 1. The total force on the boundary vanishes

$$\int_S B_x \, B_z dx dy = \int_S B_y \, B_z dx dy = 0 \tag{43}$$

$$\int_S (B_x^2 + B_y^2) dx dy = \int_S B_z^2 dx dy. \tag{44}$$

[60] 2. The total torque on the boundary vanishes

$$\int_S x(B_x^2 + B_y^2) dx dy = \int_S x B_z^2 dx dy, \tag{45}$$

$$\int_S y(B_x^2 + B_y^2) dx dy = \int_S y B_z^2 dx dy, \tag{46}$$

$$\int_S y B_x B_z dx dy = \int_S x B_y B_z dx dy. \tag{47}$$

[61] In an earlier review, *Aly* [1989] has mentioned already that the magnetic field is probably not force-free in the photosphere, where **B** is measured because the plasma β in the photosphere is of the order of 1 and pressure and gravity forces are not negligible. The integral relations (43)−(47) are not satisfied in this case in the photosphere and the measured photospheric field is not a suitable boundary condition for a force-free extrapolation. *Metcalf et al.* [1995] concluded that the solar magnetic field is not force-free in the photosphere, but becomes force-free only at about 400 km above the photosphere. *Gary* [2001] pointed out that care has to be taken when extrapolating the coronal magnetic field as a force-free field from photospheric measurements, because the force-free low corona is sandwiched between two regions (photosphere and higher

corona) with a plasma $\beta \approx 1$, where the force-free assumption might break down. An additional problem is that measurements of the photospheric magnetic vector field contain inconsistencies and noise. In particular the transverse components (say B_x and B_y) of current vector magnetographs include uncertainties.

[62] The force-free field in a domain requires the Maxwell stress (43)−(47) to sum to zero over the boundary. If these conditions are not fulfilled a force-free field cannot be found in the volume. A faithful algorithm should therefore have the capability of rejecting a prescription of the vector field at the boundary that fails to produce zero net Maxwell stress. A simple way to incorporate these conditions would be to evaluate the integrals (43)−(47) within or prior to the NLFFF computation and to refuse the vector field if the conditions are not fulfilled with sufficient accuracy. Current codes do run, however, although if fed with inconsistent boundary data, but they certainly cannot find a force-free solution in this case (because it does not exist). This property of current codes does, however, not challenge the trustworthiness of the algorithms, because the force-free and solenoidal conditions are checked in 3D, for example, with the help of the functional L as defined in (28). A non zero value of L (within numerical accuracy) tells the user that a force-free state has not been reached. In principle it would be possible that the codes do refuse to output the magnetic field in this case. For current codes this is not automatically controlled but responsibility of the user.

[63] Unfortunately current measurements of the magnetic field vector are only available routinely in the photosphere, where we have a finite β plasma and nonmagnetic forces might become important. The force-free compatibility conditions (43)−(47) are not fulfilled in the photosphere, but they should be fulfilled in the low β chromospheric and coronal plasma above. The question is if we still can use the photospheric measurements to find suitable consistent boundary conditions for a nonlinear force-free modeling. Such an approach has been called preprocessing of vector magnetograms.

3.2. Preprocessing

[64] The preprocessing routine has been developed by *Wiegelmann et al.* [2006b]. The integral relations (43)−(47) have been used to define a 2D functional of quadratic forms:

$$L_{\text{prep}} = \mu_1 L_1 + \mu_2 L_2 + \mu_3 L_3 + \mu_4 L_4, \tag{48}$$

where

$$L_1 = \left[\left(\sum_p B_x \, B_z \right)^2 + \left(\sum_p B_y \, B_z \right)^2 + \left(\sum_p B_z^2 - B_x^2 - B_y^2 \right)^2 \right], \tag{49}$$

$$L_2 = \left[\left(\sum_p x(B_z^2 - B_x^2 - B_y^2) \right)^2 + \left(\sum_p y(B_z^2 - B_x^2 - B_y^2) \right)^2 \right. $$
$$\left. + \left(\sum_p y B_x \, B_z - x B_y \, B_z \right)^2 \right], \tag{50}$$

$$L_3 = \left[\sum_p (B_x - B_{xobs})^2 + \sum_p (B_y - B_{yobs})^2 + \sum_p (B_z - B_{zobs})^2 \right],$$
(51)

$$L_4 = \left[\sum_p (\Delta B_x)^2 + (\Delta B_y)^2 + (\Delta B_z)^2 \right].$$
(52)

The surface integrals are here replaced by a summation $\sum_p$ over all grid nodes p of the bottom surface grid and the differentiation in the smoothing term is achieved by the usual five-point stencil for the 2D-Laplace operator. Each constraint L_n is weighted by a yet undetermined factor μ_n. The first term ($n = 1$) corresponds to the force-balance conditions (43)–(44), the next ($n = 2$) to the torque-free condition (45)–(47). The following term ($n = 3$) ensures that the optimized boundary condition agrees with the measured photospheric data and the last terms ($n = 4$) controls the smoothing. The 2D-Laplace operator is designated by Δ. The aim of the preprocessing procedure is to minimize L_{prep} so that all terms L_n if possible are made small simultaneously. A strategy on how to find the optimal yet undefined parameters μ_n is described by *Wiegelmann et al.* [2006b]. As result of the preprocessing we get a data set which is consistent with the assumption of a force-free magnetic field in the corona but also as close as possible to the measured data within the noise level.

4. Code Testing and Code Comparisons

4.1. Code Testing

[65] Newly developed codes for the extrapolation of nonlinear force-free fields from boundary data have to be tested before they are applied to measurements. In principle any analytical or numerically created solution of the force-free equations (1)–(3) can be used as a reference case. One cuts a plane (artificial photosphere, bottom boundary) out of the 3D reference solution (for the pure task of code testing it is also acceptable to use all six boundaries of the reference solution; these kind of data are not available for real solar cases of course) and uses the above described extrapolation codes to reconstruct the magnetic field. The result of this extrapolation is then compared with the reference to rate the quality of the reconstruction. Unfortunately, it is very hard to find a truly nonlinear 3D solution of (1)–(3) analytically and very few solutions are known. *Low and Lou* [1990] (LL) found a class of solutions which have become a standard reference for testing NLFFF extrapolation codes. LL found axisymmetric equilibria which are separable in spherical coordinates. They are self-similar in the radial coordinate, and the polar angle dependence is determined from a nonlinear eigenvalue equation. The symmetry is broken by cutting out a rectangular chunk of the solution by using a Cartesian coordinate system which is shifted and rotated with respect to the original coordinate system in which the LL equilibria are calculated. The parameters of the LL solutions and the parameters of the new Cartesian coordinate system allow for a large number of different situations which can be used for tests. The original axisymmetric spherical LL solution has also been

used (with and without symmetry breaking by shifting the origin of the coordinate system) to test spherical NLFFF programs. To our knowledge all recent implementations of the described NLFFF approaches have been tested with LL, either immediately in the original code-describing papers or in subsequent works, for example, in a blind-algorithm test within the NLFFF consortium, as described below.

[66] The MHD relaxation method and the optimization approach have been compared by *Wiegelmann and Neukirch* [2003]. Both methods have been applied to the *Low and Lou* [1990] equilibrium with exactly the same finite difference grid. The iterative equations for MHD relaxation and optimization have both the form $\frac{\partial \mathbf{B}}{\partial t} = \mu \mathbf{F}$ but the structure of $\mathbf{F}$ is more complicated for optimization than for MHD relaxation. The MHD relaxation term is indeed identical with the first term of the optimization approach. While MHD relaxation minimizes only the Lorentz force, the optimization does additional minimize $\nabla \cdot \mathbf{B}$, while a decreasing magnetic field divergence during MHD relaxation [as shown by *Wiegelmann and Neukirch*, 2003] is the result of numerical diffusion. Despite the numerical overhead in computing $\mathbf{F}$ for the optimization code, optimization provided more accurate results and faster convergence.

[67] A practical advantage of the MHD approach is that several time-dependent MHD codes are well known and established and can be used for the force-free relaxation discussed here. The inclusion of nonmagnetic forces like pressure gradients and gravity looks straight forward for the MHD approach. Other methods are usually developed with the only task of computing nonlinear force-free coronal magnetic fields, also a generalization toward magnetohydrostatic and stationary MHD equilibria is possible and has been done for the optimization approach [see *Wiegelmann and Inhester*, 2003; *Wiegelmann and Neukirch*, 2006]. Another advantage of using time-dependent MHD codes for relaxation is that the computed force-free equilibrium can be used on the same grid and with the same code as initial state for time-dependent MHD simulations. One can, in principle, use the force-free equilibria computed with any of the described method as initial state for time-dependent MHD simulation, but having the initial equilibrium state already directly on the MHD grid might be very handy, because no further adjustments are needed.

4.2. NLFFF Consortium

[68] Since the year 2004 activities are ongoing to bring NLFFF modelers together and to compare the different existing codes. A workshop series has been organized for this aim by Karel Schrijver and three workshops took place so far from 2004–2006. The next workshop is planed for June 2007. As we have been asked to summarize the workshop results on the CSWM meeting, we give also a very brief overview in the corresponding special issue paper here. The main results of the first two workshops have been published by *Schrijver et al.* [2006]. In this paper six different NLFFF implementations (Grad-Rubin codes of *Amari et al.* [1999] and *Wheatland* [2004], MHD relaxation code of *Valori et al.* [2005], optimization codes by McTiernan and by *Wiegelmann* [2004], boundary element method by *Yan and Sakurai* [2000]) have been compared. The codes have been tested in a blind algorithm test with the help of the semianalytic equilibrium by *Low and Lou* [1990]

in two cases. In case I all six boundaries of a computational box have been described, and in case II only the bottom boundary has been described. The comparison of the extrapolation results with the reference solution has been done qualitatively by magnetic field line plots (shown here in Figure 3 for the central region of case II) and quantatively by a number of sophisticated comparison matrices. All NLFFF fields agreed best with the reference field for the low-lying central magnetic field region, where the magnetic field and electric currents are strongest and the influence of the boundaries lowest. The code converged with speeds that differed by a factor of one million per iteration steps. (The codes run on different machines, have been written in different programming languages and used different compilers. A real test of the exact computing time would comprise a proper operation count, for example, the number of fixed point additions and multiplications per iteration step.) The fastest-converging and best-performing code was the *Wheatland et al.* [2000] optimization code as implemented by *Wiegelmann* [2004]. Recent implementations of the Grad-Rubin code by *Amari et al.* [2006] and *Inhester and Wiegelmann* [2006] and a new implementation of the upward integration method by *Song et al.* [2006] did not participate in the blind-algorithm intercomparison by *Schrijver et al.* [2006], but these three new codes have been tested by the authors with similar measures and revealed similar accuracy as the best performing codes in the blind algorithm test. It seems that the somewhat more flexible boundary conditions used in the Grad-Rubin approaches of *Amari et al.* [2006] and *Inhester and Wiegelmann* [2006] are responsible for the better performance compared to the earlier implementation by *Amari et al.* [1999], which has been used in the blind algorithm test.

[69] The widely used LL equilibrium contains a very smooth photospheric magnetic field and an extended current distribution. It is therefore also desirable to test NLFFF codes also with other, more challenging boundary fields, which are less smooth, have localized current distribution and to investigate also the effects of noise and effects from non-force-free boundaries. A somewhat more challenging reference case is the equilibrium found by *Titov and Démoulin* [1999] (TD). Similar to LL, the TD equilibrium is an axisymmetric equilibrium. The TD model contains a potential field which is disturbed by a toroidal nonlinear force-free current. This equilibrium has been used for testing the MHD relaxation code (G. Valori and B. Kliem, personal communication, 2006) and the optimization code from *Wiegelmann et al.* [2006a].

[70] Any numerically created NLFFF model might be suitable for code testing, too. It is in particular interesting to use models, which are partly related on observational data. Very recently, *van Ballegooijen et al.* [2007] used line-of-sight photospheric measurements from SOHO/MDI to compute a potential field, which was then disturbed by inserting a twisted flux robe and relaxed toward a nonlinear force-free state with a magnetofrictional method as described by *van Ballegooijen* [2004]. The *van Ballegooijen et al.* [2007] model is not force-free in the entire computational domain, but only above a certain height above the bottom boundary (artificial chromosphere). On the lowest boundary (photosphere) the model contains significant nonmagnetic forces. Both the chromospheric as well as the photospheric mag-

netic field vector from the *van Ballegooijen et al.* [2007] model have been used to test four of the recently developed extrapolation codes (one Grad-Rubin method, one MHD relaxation code and two optimization approaches) in a second blind algorithm test by *Metcalf et al.* [2007]. While the NLFFF consortium paper, part I [*Schrijver et al.*, 2006], used a domain of just 64^3 pixel, the part II paper used a computational domain of $320 \times 320 \times 258$ pixel and modern NLFFF codes where able to compute the nonlinear force-free field in such relatively large boxes within a few hours for a moderate parallelization on only 1–4 processors and a memory requirement of 2.5–4 GB of RAM. This very recent code comparison shows a major improvement regarding computing time and suitable grid sizes within less than 3 years. On the first NLFFF consortium meeting in 2004, box sizes of some 64^3 have been a kind of standard or computing times of some 2 weeks have been reported for 150^3 boxes. We briefly summarize the results of *Metcalf et al.* [2007] as: (1) NLFFF extrapolations from chromospheric data recover the original reference field with high accuracy; (2) when the extrapolations are applied to the photospheric data, the reference field is not well recovered; and (3) preprocessing of the photospheric data improve the result, but the accuracy is still lower as for extrapolations from the chromosphere.

5. Conclusions and Outlook

[71] Within the last few years the scientific community showed a growing interest into coronal magnetic fields. (Publications containing the phrase 'coronal magnetic fields' in title or abstract have been cited less than about 50 times per year until the early 1990s and this number increased to about 150 citations per year in 2004. A peak year was 2006 (last year) with more than 300 citations (source: ISI Web of Knowledge, March 2007)). The development of new ground based and space born vector magnetographs provide us measurements of the magnetic field vector on the suns photosphere. Accompanied from these hardware development, software has been developed to extrapolate the photospheric measurements into the corona. Special attention has recently been given to nonlinear force-free codes. Five different numerical approaches (Grad-Rubin, upward integration, MHD relaxation, optimization, boundary elements) have been developed for this aim. It is remarkable that new codes or major updates of existing codes have been published for all five methods within the last two years, mainly in the last year (2006). A workshop series (NLFFF consortium) since 2004 on nonlinear force-free fields has recently released synergy effects, by bringing modelers of the different numerical implementations together to compare, evaluate and improve the programs. Several of the most recent new codes and utility programs (e.g., preprocessing) have at least been partly inspired by these workshops. The new implementations have been tested with the smooth semianalytic Low-Lou equilibrium and showed reasonable agreement with this reference field. While all methods aim for a reconstruction of the coronal magnetic field from the photospheric magnetic field vector, the way how these measurements are used to prescribe the boundaries of the codes is different.
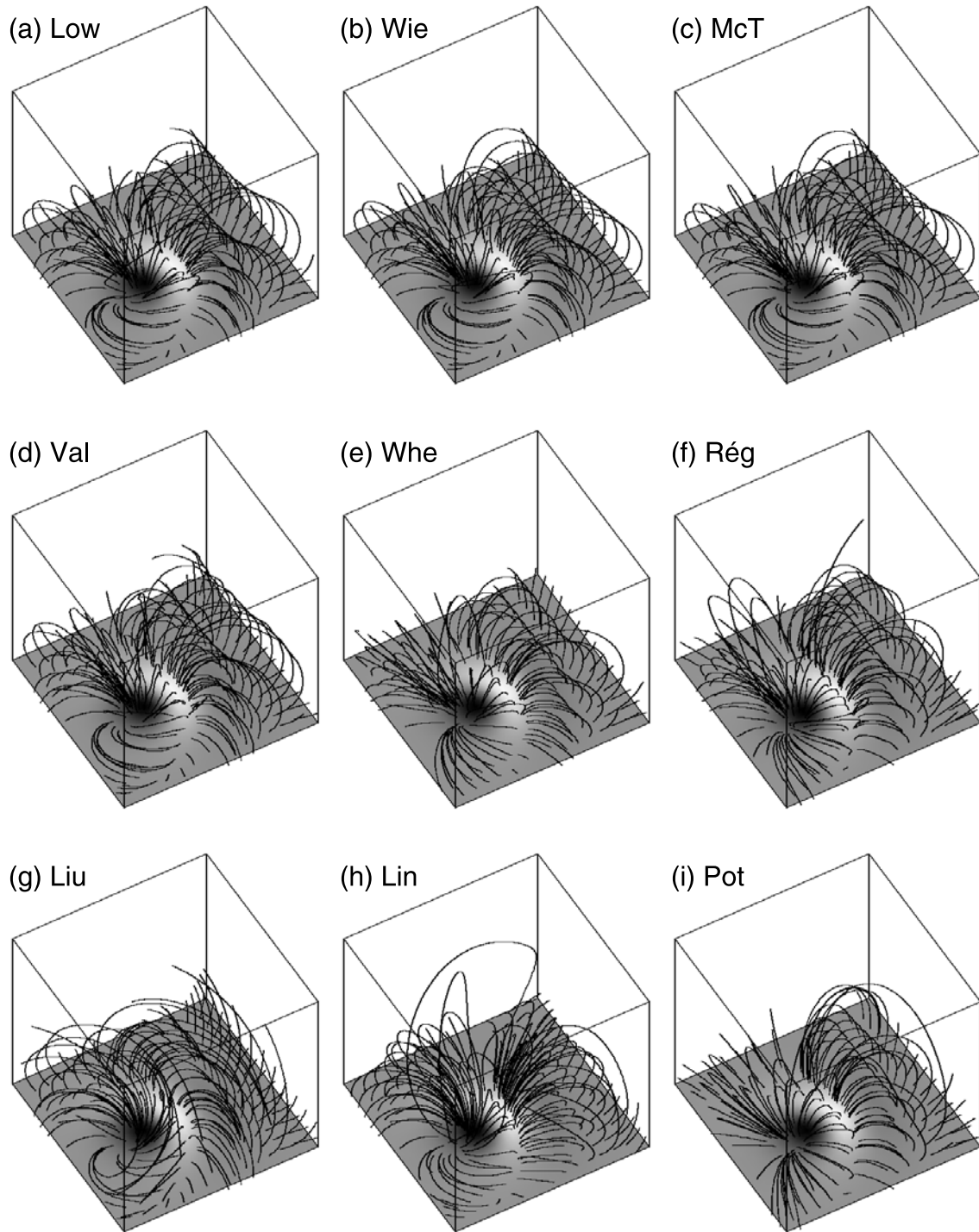
Figure 3. Evaluation of six nonlinear force−free codes. The (a) reference solution has been compared with extrapolations with (b, c) optimation, (d) MHD relaxation, (e, f) Grand−Rubin, and (g) boundary element. For comparison, (h) linear-force-free and (i) potential fields are shown, too. The images show the central domain of the model. Only the bottom boundary has been provided for the extrapolation. (This figure was originally published as *Schrijver et al.*'s [2006] Figure 4. Used with permission of Springer.)

[72]   1. MHD relaxation and optimization use B_{x0}, B_{y0}, B_{z0} on the bottom boundary. This overdetermines the boundary value problem. Both methods are closely related and compute the magnetic field in a computational box with

$$\frac{\partial \mathbf{B}}{\partial t} = \mu \mathbf{F},   (53)$$

where the structure of $\mathbf{F}$ is somewhat different (the optimization approach has more terms) for both methods. Usually a potential field is used as initial state for both approaches, also the use of a linear force-free initial state is possible. Recently a multiscale version of optimization has been installed, which uses a low-resolution NLFFF field as input for higher-resolution computations. Specifying the entire magnetic field vector on the bottom boundary is an overimposed problem and a unique NLFFF field (or a solution at all) requires that the boundary data fulfill certain consistency criteria. A recently developed preprocessing routine helps to find suitable consistent boundary data from inconsistent photospheric measurements. Earlier and current comparisons showed a somewhat higher accuracy for the optimization approach. A practical advantage of the MHD approach is that in principle any available time-dependent MHD code can be adjusted to compute the NLFFF field.

[73]   2. The Grad-Rubin approach uses B_{z0} and the distribution of α computed with equation (8) for one polarity, which corresponds to well posed mathematical problem. A practical problem is that the computation of α requires numerical differences of the noisy and forced transverse photospheric field B_{x0}, B_{y0} with (7) leading to inaccuracies in the normal electric current distribution and in α. For smooth semianalytic test cases this is certainly not a problem, but real data require special attention (smoothing, preprocessing, limiting $\alpha \neq 0$ to regions where B_{z0} is above a certain limit) to derive a meaningful distribution of α. While the method requires only α for one polarity, the computation from photospheric data provide α for both polarities. We are not aware of any tests on how well NLFFF solutions computed from α prescribed on the positive and negative polarity coincide. It is also unclear how well the computed transverse field components on the bottom boundary agree with the measured values of B_{x0}, B_{y0}. (In principle B_{x0}, B_{y0} may have an additional field $(B_{x0}, B_{y0}) + (\partial_x \partial_y) \varphi$ without making a difference for α and hence for the Grad-Rubin result.) More tests on this topics are necessary, including the recently installed possibility to prescribe α for both polarities and adjust the boundary by a weighed average of α on both polarities to fulfill equation (6). As initial state the Grad-Rubin method uses a potential field, which is also true for MHD relaxation and optimization.

[74]   3. The upward integration and the boundary element method prescribe both all components of the bottom boundary magnetic field vector and the α distribution computed with equation (8). This approach over imposes the boundary and B_{x0}, B_{y0}, B_{z0} and α have to be consistent which each other and the force-free assumption. This is certainly not a problem at all for smooth semianalytic test equilibria and strategies to derive consistent boundary data from measured data have been developed recently. Different from the three

approaches discussed above, upward integration and boundary element methods do not require to compute first an initial potential field in the computational domain. It is well known that the upward integration method is based on an ill-posed problem and the method has not been considered for several years, but a recent implementation with smooth analytic functions might help to regularize this method. First tests showed a reasonable results for computations with the smooth semianalytic Low-Lou solution.

[75]   The boundary element method has the problem to be very slow and an earlier implementation of this method could not reach a converged state for a 64^3 boxed used in the NLFFF consortium paper, part I, owing to this problem. A new 'direct boundary method' has been developed, which seems to be faster than the original 'boundary element method', but still slower compared with the four other NLFFF approaches if the task is to compute a 3D magnetic field in an entire 3D domain. Different from all other described methods the boundary element approach allows to compute the nonlinear force-free field vector at any arbitrary point above the boundary and it is not necessary to compute the entire 3D field above the photosphere. This might be a very useful feature if one is interested in computing the magnetic field only along a single loop and not interested in an entire active region.

[76]   The new implementations of upward integration and boundary element method show both reasonable results for first tests with the smooth semianalytic Low and Lou equilibrium. Further tests with more sophisticated equilibria, for example, a solar-like test case as used in the NLFFF consortium paper, part II, would be useful to come to more sound conclusions regarding the feasibility of these methods.

[77]   Most of the efforts done in nonlinear force-free modeling until now concentrated mainly on developing these models and testing their accuracy and speed with the help of well known test configuration. Not too many applications of nonlinear force-free models to real data are currently available, from which we learned new physics. One reason was the insufficient access to high-accuracy photospheric vector magnetograms and a second one were limitations of the models. Force-free field extrapolation is a mere tool, if properly employed on vector magnetograms, it can help to understand physical, magnetic field dominated processes in the corona. Both the computational methods as well as the accuracy of required measurements (e.g., with Hinode, SDO) are rapidly improving. Within the NLFFF consortium we just started (since April 2007) to apply the different codes to compute nonlinear force-free coronal magnetic fields from Hinode vectormagnetograms. This project might provide us already some new insights about coronal physics.

[78]   To conclude, we can say that the capability of Cartesian nonlinear force-free extrapolation codes has rapidly increased in recent years. Only 3 years ago most codes run usually on grids of about 64^3 pixel. Recently developed or updated codes (Grad-Rubin by Wheatland, MHD relaxation by Valori, optimization by Wiegelmann, optimization by McTiernan) have been applied to grids of about 300^3 pixel. Although this increase of traceable grid sizes is certainly encouraging, the resolution of current and near-

future vector magnetographs (which of course measure only data in 2D!) is significantly higher. We should keep in mind, however, that the currently implemented NLFFF codes have been only moderately parallelized using only a few processors. The CSWM conference, where this paper has been presented, took place at the 'Earth simulator' in Yokohama, which contains several thousands of processors used for Earth-science computer simulations. An installation of NLFFF codes on such massive parallel computers (which has been briefly addressed on NLFFF consortium meetings) combined with adaptive mesh refinements might enable drastically improved grid sizes. One should not underestimate the time and effort necessary to program and install such massive parallelized versions of existing codes. As full disk vectormagnetograms will become available soon (SOLIS, SDO/HMI) it is also an important task to take a spherical geometry into account. First steps in this direction have been carried out with the optimization and boundary element methods. Spherical NLFFF geometries are currently still in it's infancy and have been tested until now only with smooth semianalytic Low and Lou equilibria and require further developments.

[79] Attention has also recently been drawn to the problem that the coronal magnetic field is force-free, but the photospheric one is not. Tests with extrapolations from solar-like artificial photospheric and chromospheric measurements within the NLFFF consortium paper, part II, revealed that extrapolations from the (force-free) chromospheric field provide significantly better results as extrapolations using directly the (forced) photospheric field. Applying a preprocessing program on the photospheric data, which effectively removes the nonmagnetic forces, leads to significantly better results, but they are not as good as by using the chromospheric magnetic field vector as boundary condition. An area of current research is the possibility to use chromospheric images to improve the preprocessing of photospheric magnetic field measurements. Improvements in measuring the chromospheric magnetic field directly [e.g., *Lagg et al.*, 2004] might further improve to find suitable boundary conditions for NLFFF extrapolations. Force-free extrapolations are not suitable, however, to understand the details of physical processes on how the magnetic field evolves from the forced photosphere into the chromosphere, because nonmagnetic forces are important in the photosphere. For a better understanding of these phenomena more sophisticated models which take pressure gradients and gravity (and maybe also plasma flow) into account are required. Some first steps have been done with a generalization of the optimization method by *Wiegelmann and Neukirch* [2006], but such approaches are still in their infancy and have been tested so far only with smooth MHD equilibria. It is also not entirely clear how well necessary information regarding the plasma (density, pressure, temperature, flow) can be derived from measurements. Nonmagnetic forces become important also in quiet sun regions [*Schrijver and van Ballegooijen*, 2005] and in the higher layers of the corona, where the plasma β is of the order of unity. Coronagraph measurements, preferably from two viewpoints as provided by the STEREO mission, combined with a tomographic inversion might help here to get insights in the required 3D structure of the plasma density. One should also pay attention to the combination of extrapolation methods, as described here, with measurements of the Hanle and Zeeman effects in coronal lines which allows the reconstruction of the coronal magnetic field as proposed in feasibility studies of vector tomography by *Kramar et al.* [2006] and *Kramar and Inhester* [2006]. Other measurements of coronal features, for example, coronal plasma images from two STEREO viewpoints, can be used for observational tests of coronal magnetic field models. Using two viewpoints provide a much more restrictive test of models as images from only one view direction. While a nonlinear force-free coronal magnetic field model helps us to derive the topology, magnetic field and electric current strength in coronal loops, they do not provide plasma parameters. One way to get insights regarding the coronal plasma is the use of scaling laws to model the plasma along the reconstructed 3D field lines and compare correspondent artificial plasma images with real coronal images. *Schrijver et al.* [2004] applied such an approach to global potential coronal magnetic fields and compared simulated and real coronal images from one viewpoint. A generalization of such methods toward the use of more sophisticated magnetic field models and coronal images from two STEREO viewpoints will probably provide many insights regarding the structure and physics of the coronal plasma. An important challenge is for example the coronal heating problem. The dominating coronal magnetic field is assumed to play an important role here, because magnetic field configuration containing free energy can under certain circumstances reconnect *Priest* [1996, 1999] and supply energy for coronal heating. *Priest et al.* [2005] pointed out that magnetic reconnection at separators and separatrices plays an important role for coronal heating. Nonlinear force-free models can help here to identify the magnetic field topology, magnetic null points, separatrices and localized strong current concentration. While magnetic reconnection [see, e.g., *Priest and Schrijver*, 1999] is a dynamical phenomenon, the static magnetic field models discussed here can help to identify the locations favorable for reconnection. Time sequences of nonlinear force-free models computed from corresponding vector magnetograms will also tell wether the topology of the coronal magnetic field has changed due to reconnection, even if the physics of reconnection is not described by force-free models. Sophisticated 3D coronal magnetic field models and plasma images from two viewpoints might help to constrain the coronal heating function further, which has been done so far with plasma images from one viewpoint [*Aschwanden*, 2001a, 2001b] (by using data from Yokoh, Soho and Trace).

References

Alissandrakis, C. E. (1981), On the computation of constant alpha force-free magnetic field, *Astron. Astrophys.*, *100*, 197–200.

Aly, J. J. (1984), On some properties of force-free magnetic fields in infinite regions of space, *Astrophys. J.*, *283*, 349–362, doi:10.1086/162313.

Aly, J. J. (1989), On the reconstruction of the nonlinear force-free coronal magnetic field from boundary data, *Sol. Phys.*, *120*, 19–48.

Aly, J. J. (2005), A uniqueness result for a simple force-free magnetic field submitted to a topological constraint, *Astron. Astrophys.*, *429*, 15–18, doi:10.1051/0004-6361:20041547.

Amari, T., J. J. Aly, J. F. Luciani, T. Z. Boulmezaoud, and Z. Mikic (1997), Reconstructing the solar coronal magnetic field as a force-free magnetic field, *Sol. Phys.*, *174*, 129–149.

Amari, T., T. Z. Boulmezaoud, and Z. Mikic (1999), An iterative method for the reconstructionbreak of the solar coronal magnetic field. I. Method for regular solutions, *Astron. Astrophys.*, *350*, 1051–1059.

Amari, T., T. Z. Boulmezaoud, and J. J. Aly (2006), Well posed reconstruction of the solar coronal magnetic field, Astron, *Astrophys.*, *446*, 691–705, doi:10.1051/0004-6361:20054076.

Aschwanden, M. J. (2001a), Revisiting the determination of the coronal heating function from Yohkoh data, *Astrophys. J.*, *559*, L171–L174, doi:10.1086/323788.

Aschwanden, M. J. (2001b), An evaluation of coronal heating models for active regions based on Yohkoh, SOHO, and TRACE observations, *Astrophys. J.*, *560*, 1035–1044, doi10.1086/323064.

Aschwanden, M. J. (2005), *Physics of the Solar Corona: An Introduction with Problems and Solutions*, 2nd ed., Springer, New York.

Aschwanden, M. J., J. S. Newmark, J.-P. Delaboudinière, W. M. Neupert, J. A. Klimchuk, G. A. Gary, F. Portier-Fozzani, and A. Zucker (1999), Three-dimensional stereoscopic analysis of solar active region loops. I. SOHO/EIT observations at temperatures of $(1.0–1.5) \times 10^6$ K, *Astrophys. J.*, *515*, 842–867, doi:10.1086/307036.

Bineau, M. (1972), Existence of force-free magnetic-fields, *Commun. Pure Appl. Math.*, *25*, 77–84.

Bleybel, A., T. Amari, L. van Driel-Gesztelyi, and K. D. Leka (2002), Global budget for an eruptive active region. I. Equilibrium reconstruction approach, *Astron. Astrophys.*, *395*, 685–695, doi:10.1051/0004-6361:20021332.

Borrero, J. M., S. Tomczyk, A. Norton, T. Darnell, J. Schou, P. Scherrer, R. Bush, and Y. Lui (2006), Magnetic field vector retrieval with HMI, in *Solar Polarization 4, ASP Conf. Ser.*, vol. 358, edited by R. Casini and B. W. Lites, p. 144, Astron. Soc. of the Pac., San Francisco, Calif. (Available at http://arxiv.org/abs/astro-ph/0602130)

Bossavit, A. (1988), Mixed finite elements and the complex of Whitney forms, in *The Mathematics of Finite Elements and Applications VI*, edited by J. Whiteman, pp. 137–144, Academic Press, London.

Boulmezaoud, T. Z., and T. Amari (2000), On the existence of non-linear force-free fields in three-dimensional domains, *ZAMP*, *51*, 942–967.

Carcedo, L., D. S. Brown, A. W. Hood, T. Neukirch, and T. Wiegelmann (2003), A quantitative method to optimise magnetic field line fitting of observed coronal loops, *Sol. Phys.*, *218*, 29–40.

Chiu, Y. T., and H. H. Hilton (1977), Exact Green's function method of solar force-free magnetic-field computations with constant alpha. I. Theory and basic test cases, *Astrophys. J.*, *212*, 873–885.

Chodura, R., and A. Schlueter (1981), A 3D code for MHD equilibrium and stability, *J. Comput. Phys.*, *41*, 68–88.

Cuperman, S., L. Ofman, and M. Semel (1990), Extrapolation of photospheric potential magnetic fields using oblique boundary values—A simplified approach, *Astron. Astrophys.*, *227*, 583–590.

Cuperman, S., P. Demoulin, and M. Semel (1991), Removal of singularities in the Cauchy problem for the extrapolation of solar force-free magnetic fields, *Astron. Astrophys.*, *245*, 285–288.

Dedner, A., F. Kemm, D. Kröner, C.-D. Munz, T. Schnitzer, and M. Wesenberg (2002), Hyperbolic divergence cleaning for the MHD equations, *J. Comput. Phys.*, *175*, 645–673.

Demoulin, P., and E. R. Priest (1992), The properties of sources and sinks of a linear force-free field, *Astron. Astrophys.*, *258*, 535–541.

Gary, G. A. (2001), Plasma Beta above a solar active region: Rethinking the paradigm, *Sol. Phys.*, *203*, 71–86.

Gary, G. A., and M. J. Hagyard (1990), Transformation of vector magnetograms and the problems associated with the effects of perspective and the azimuthal ambiguity, *Sol. Phys.*, *126*, 21–36.

Grad, H., and H. Rubin (1958), Hydromagnetic equilibria and force-free fields, paper presented at 2nd International Conference on Peaceful Uses of Atomic Energy, Int. At. Energy Agency, Geneva.

He, H., and H. Wang (2006), The validity of the boundary integral equation for magnetic field extrapolation in open space above a spherical surface, *Mon. Not. R. Astron. Soc.*, *369*, 207–215, doi:10.1111/j.1365-2966.2006.10288.x.

Henney, C. J., C. U. Keller, and J. W. Harvey (2006), SOLIS-VSM solar vector magnetograms, in *Solar Polarization 4, ASP Conf. Ser.*, vol. 358, edited by R. Casini and B. W. Lites, p. 92, Astron. Soc. of the Pac., San Francisco, Calif. (Available at http://arxiv.org/abs/astro-ph/0701122)

Inhester, B., and T. Wiegelmann (2006), Nonlinear force-free magnetic field extrapolations: Comparison of the Grad Rubin and Wheatland Sturrock Roumeliotis algorithm, *Sol. Phys.*, *235*, 201–221, doi:10.1007/s11207-006-0065-x.

Jiao, L., A. N. McClymont, and Z. Mikic (1997), Reconstruction of the three-dimensional coronal magnetic field, *Sol. Phys.*, *174*, 311–327.

Judge, P. G. (1998), Spectral lines for polarization measurements of the coronal magnetic field. I. Theoretical intensities, *Astrophys. J.*, *500*, 1009–1022.

Kageyama, A., and T. Sato (2004), "Yin-Yang grid": An overset grid in spherical geometry, *Geochem. Geophys. Geosyst.*, *5*, Q09005, doi:10.1029/2004GC000734.

Keppens, R., M. Nool, G. Tóth, and J. P. Goedbloed (2003), Adaptive mesh refinement for conservative systems: Multi-dimensional efficiency evaluation, *Comput. Phys. Commun.*, *153*, 317–339.

Klimchuk, J. A., and P. A. Sturrock (1992), Three-dimensional force-free magnetic fields and flare energy buildup, *Astrophys. J.*, *385*, 344–353, doi:10.1086/170943.

Kramar, M., and B. Inhester (2006), Inversion of coronal Zeeman and Hanle observations to reconstruct the coronal magnetic field, *Mem. Soc. Astron. Ital.*, *78*, 120. (Available at http://arxiv.org/abs/astro-ph/0612639)

Kramar, M., B. Inhester, and S. K. Solanki (2006), Vector tomography for the coronal magnetic field. I. Longitudinal Zeeman effect measurements, *Astron. Astrophys.*, *456*, 665–673, doi:10.1051/0004-6361:20064865.

LaBonte, B. J., D. L. Mickey, and K. D. Leka (1999), The imaging vector magnetograph at Haleakalā: II. Reconstruction of Stokes spectra, *Sol. Phys.*, *189*, 1–24.

Lagg, A., J. Woch, N. Krupp, and S. K. Solanki (2004), Retrieval of the full magnetic vector with the He I multiplet at 1083 nm: Maps of an emerging flux region, *Astron. Astrophys.*, *414*, 1109–1120.

Leka, K. D., and A. Skumanich (1999), On the value of 'αAR' from vector magnetograph data: I. Methods and caveats, *Sol. Phys.*, *188*, 3–19.

Li, Z., Y. Yan, and G. Song (2004), Properties of the boundary integral equation for solar non-constant-α force-free magnetic fields, *Mon. Not. R. Astron. Soc.*, *347*, 1255–1265, doi:10.1111/j.1365-2966.2004.07309.x.

Lin, H., J. R. Kuhn, and R. Coulter (2004), Coronal magnetic field measurements, *Astrophys. J. Lett.*, *613*, L177–L180, doi:10.1086/425217.

Liu, Y., X. P. Zhao, J. T. Hoeksema, P. H. Scherrer, J. Wang, and Y. Yan (2002), On formation of the sigmoidal structure in solar active region NOAA 8100, *Sol. Phys.*, *206*, 333–346.

Low, B. C., and Y. Q. Lou (1990), Modeling solar force-free magnetic fields, *Astrophys. J.*, *352*, 343–352.

McClymont, A. N., L. Jiao, and Z. Mikic (1997), Problems and progress in computing three-dimensional coronal active region magnetic fields from boundary data, *Sol. Phys.*, *174*, 191–218.

Metcalf, T. R. (1994), Resolving the 180-degree ambiguity in vector magnetic field measurements: The 'minimum' energy solution, *Sol. Phys.*, *155*, 235–242.

Metcalf, T. R., L. Jiao, A. N. McClymont, R. C. Canfield, and H. Uitenbroek (1995), Is the solar chromospheric magnetic field force-free?, *Astrophys. J.*, *439*, 474–481, doi:10.1086/175188.

Metcalf, T. R., et al. (2006), An overview of existing algorithms for resolving the 180-degree ambiguity in vector magnetic fields: Quantitative tests with synthetic data, *Sol. Phys.*, *237*, 267–296, doi:10.1007/s11207-006-0170-x.

Metcalf, T. R., M. L. DeRosa, C. J. Schrijver, G. Barnes, A. VanBallegooijen, T. Wiegelmann, M. S. Wheatland, G. Valori, and J. M. McTiernan (2007), Non-linear force-free modeling of coronal magnetic fields. II. Modeling a filament arcade from simulated chromospheric and photospheric vector fields, *Sol. Phys.*, in press.

Mickey, D. L., R. C. Canfield, B. J. Labonte, K. D. Leka, M. F. Waterson, and H. M. Weber (1996), The imaging vector magnetograph at Haleakala, *Sol. Phys.*, *168*, 229–250.

Mikic, Z., and A. N. McClymont (1994), Deducing coronal magnetic fields from vector magnetograms, in *Solar Active Region Evolution: Comparing Models with Observations, ASP Conf. Ser.*, vol. 68, edited by K. S. Balasubramaniam and G. W. Simon, pp. 225-232, Astron. Soc. of the Pac., San Francisco, Calif.

Mikic, Z., D. C. Barnes, and D. D. Schnack (1988), Dynamical evolution of a solar coronal magnetic field arcade, *Astrophys. J.*, *328*, 830–847, doi:10.1086/166341.

Molodensky, M. M. (1969), Integral properties of force-free fields, *Soviet Astron., Engl. Transl.*, *12*, 585–588.

Molodensky, M. M. (1974), Equilibrium and stability of force-free magnetic field, *Sol. Phys.*, *39*, 393–404.

Nakagawa, Y. (1974), Dynamics of the solar magnetic field. I. Method of examination of force-free magnetic fields, *Astrophys. J.*, *190*, 437–440.

Nakagawa, Y., and M. A. Raadu (1972), On practical representation of magnetic field, *Sol. Phys.*, *25*, 127–135.

Pevtsov, A. A., R. C. Canfield, and T. R. Metcalf (1994), Patterns of helicity in solar active regions, *Astrophys. J. Lett.*, *425*, L117–L119, doi:10.1086/187324.

Press, W. H. (2002), *Numerical Recipes in C++: The Art of Scientific Computing*, 1002 pp., Cambridge Univ. Press, New York.

Priest, E. (1996), Coronal heating by magnetic reconnection, *Astrophys. Space Sci.*, *237*, 49–73.

Priest, E. R. (1999), Heating the solar corona by magnetic reconnection, *Astrophys. Space Sci.*, *264*, 77–100.

Priest, E. R., and C. J. Schrijver (1999), Aspects of three-dimensional magnetic reconnection (invited review), *Sol. Phys.*, *190*, 1–24, doi:10.1023/A:1005248007615.

Priest, E. R., D. W. Longcope, and J. Heyvaerts (2005), Coronal heating at separators and separatrices, *Astrophys. J.*, *624*, 1057–1071, doi:10.1086/429312.

Régnier, S., and T. Amari (2004), 3D magnetic configuration of the Hα filament and X-ray sigmoid in NOAA AR 8151, *Astron. Astrophys.*, *425*, 345–352.

Régnier, S., and R. C. Canfield (2006), Evolution of magnetic fields and energetics of flares in active region 8210, *Astron. Astrophys.*, *451*, 319–330, doi:10.1051/0004-6361:20054171.

Régnier, S., T. Amari, and E. Kersalé (2002), 3D coronal magnetic field from vector magnetograms: Non-constant-alpha force-free configuration of the active region NOAA 8151, *Astron. Astrophys.*, *392*, 1119–1127.

Régnier, S., T. Amari, and R. C. Canfield (2005), Self and mutual magnetic helicities in coronal magnetic configurations, *Astron. Astrophys.*, *442*, 345–349, doi:10.1051/0004-6361:20053509.

Roumeliotis, G. (1996), The "stress-and-relax" method for reconstructing the coronal magnetic field from vector magnetograph data, *Astrophys. J.*, *473*, 1095–1103.

Sakurai, T. (1981), Calculation of force-free magnetic field with non constant alpha, *Sol. Phys.*, *69*, 343–359.

Sakurai, T. (1982), Green's function methods for potential magnetic fields, *Sol. Phys.*, *76*, 301–321.

Sakurai, T. (1989), Computational modeling of magnetic fields in solar active regions, *Space Sci. Rev.*, *51*, 11–48.

Sakurai, T., et al. (1995), Solar flare telescope at Mitaka, *Publ. Astron. Soc. Jpn.*, *47*, 81–92.

Schatten, K. H., J. M. Wilcox, and N. F. Ness (1969), A model of interplanetary and coronal magnetic fields, *Sol. Phys.*, *6*, 442–455.

Schmidt, H. U. (1964), On the observable effects of magnetic energy storage and release connected with solar flares, in *The Physics of Solar Flares*, edited by W. N. Hess, pp. 107–114, NASA, Washington, D. C.

Schrijver, C. J., and A. A. van Ballegooijen (2005), Is the quiet-sun corona a quasi-steady, force-free environment?, *Astrophys. J.*, *630*, 552–560, doi:10.1086/431754.

Schrijver, C. J., A. W. Sandman, M. J. Aschwanden, and M. L. DeRosa (2004), The coronal heating mechanism as identified by full-sun visualizations, *Astrophys. J.*, *615*, 512–525, doi:10.1086/424028.

Schrijver, C. J., M. L. DeRosa, A. M. Title, and T. R. Metcalf (2005), The nonpotentiality of active-region coronae and the dynamics of the photospheric magnetic field, *Astrophys. J.*, *628*, 501–513, doi:10.1086/430733.

Schrijver, C. J., M. L. Derosa, T. R. Metcalf, Y. Liu, J. McTiernan, S. Régnier, G. Valori, M. S. Wheatland, and T. Wiegelmann (2006), Nonlinear force-free modeling of coronal magnetic fields part i: A quantitative comparison of methods, *Sol. Phys.*, *235*, 161–190, doi:10.1007/s11207-006-0068-7.

Seehafer, N. (1978), Determination of constant alpha force-free solar magnetic fields from magnetograph data, *Sol. Phys.*, *58*, 215–223.

Seehafer, N. (1982), A comparison of different solar magnetic field extrapolation procedures, *Sol. Phys.*, *81*, 69–80.

Semel, M. (1967), Contribution à létude des champs magn\' etiques dans les régions actives solaires, *Ann. Astrophys.*, *30*, 513.

Semel, M. (1988), Extrapolation functions for constant-alpha force-free fields—Green's method for the oblique boundary value, *Astron. Astrophys.*, *198*, 293–299.

Shimizu, T. (2004), SolarB Solar Optical Telescope (SOT), in *The Solar-B Mission and the Forefront of Solar Physics, ASP Conf. Ser.*, vol. 325, edited by T. Sakurai and T. Sekii, p. 3, Astron. Soc. of the Pac., San Francisco, Calif.

Solanki, S. K., A. Lagg, J. Woch, N. Krupp, and M. Collados (2003), Three-dimensional magnetic field topology in a region of solar coronal heating, *Nature*, *425*, 692–695.

Song, M. T., C. Fang, Y. H. Tang, S. T. Wu, and Y. A. Zhang (2006), A new and fast way to reconstruct a nonlinear force-free field in the solar corona, *Astrophys. J.*, *649*, 1084–1092, doi:10.1086/506249.

Titov, V. S., and P. Démoulin (1999), Basic topology of twisted magnetic configurations in solar flares, *Astron. Astrophys.*, *351*, 707–720.

Török, T., and B. Kliem (2003), The evolution of twisting coronal magnetic flux tubes, *Astron. Astrophys.*, *406*, 1043–1059, doi:10.1051/0004-6361:20030692.

Valori, G., B. Kliem, and R. Keppens (2005), Extrapolation of a nonlinear force-free field containing a highly twisted magnetic loop, *Astron. Astrophys.*, *433*, 335–347.

van Ballegooijen, A. A. (2004), Observations and modeling of a filament on the Sun, *Astrophys. J.*, *612*, 519–529, doi:10.1086/422512.

van Ballegooijen, A. A., E. E. Deluca, K. Squires, and D. H. Mackay (2007), Modeling magnetic flux ropes in the solar atmosphere, *J. Atmos. Terr. Phys.*, *69*, 24–31, doi:10.1016/j.jastp.2006.06.007.

Wang, H., Y. Yan, T. Sakurai, and M. Zhang (2000), Topology of magnetic field and coronal heating in solar active regions. II. The role of quasi-separatrix layers, *Sol. Phys.*, *197*, 263–273.

Wheatland, M. S. (1999), A better linear force-free field, *Astrophys. J.*, *518*, 948–953, doi:10.1086/307301.

Wheatland, M. S. (2004), Parallel construction of nonlinear force-free fields, *Sol. Phys.*, *222*, 247–264.

Wheatland, M. S. (2006), A fast current-field iteration method for calculating nonlinear force-free fields, *Sol. Phys.*, *238*, 29–39, doi:10.1007/s11207-006-0232-0.

Wheatland, M. S., P. A. Sturrock, and G. Roumeliotis (2000), An optimization approach to reconstructing force-free fields, *Astrophys. J.*, *540*, 1150–1155.

Wiegelmann, T. (2004), Optimization code with weighting function for the reconstruction of coronal magnetic fields, *Sol. Phys.*, *219*, 87–108.

Wiegelmann, T. (2007), Computing nonlinear force-free coronal magnetic fields in spherical geometry, *Sol. Phys.*, *240*, 227–239, doi:10.1007/s11207-006-0266-3.

Wiegelmann, T., and B. Inhester (2003), Magnetic modeling and tomography: First steps towards a consistent reconstruction of the solar corona, *Sol. Phys.*, *214*, 287–312.

Wiegelmann, T., and T. Neukirch (2002), Including stereoscopic information in the reconstruction of coronal magnetic fields, *Sol. Phys.*, *208*, 233–251.

Wiegelmann, T., and T. Neukirch (2003), Computing nonlinear force free coronal magnetic fields, *Nonlinear Processes Geophys.*, *10*, 313–322.

Wiegelmann, T., and T. Neukirch (2006), An optimization principle for the computation of MHD equilibria in the solar corona, *Astron. Astrophys.*, *457*, 1053–1058, doi:10.1051/0004-6361:20065281.

Wiegelmann, T., B. Inhester, A. Lagg, and S. K. Solanki (2005a), How to use magnetic field information for coronal loop identification, *Sol. Phys.*, *228*, 67–78, doi:10.1007/s11207-005-2511-6.

Wiegelmann, T., A. Lagg, S. K. Solanki, B. Inhester, and J. Woch (2005b), Comparing magnetic field extrapolations with measurements of magnetic loops, *Astron. Astrophys.*, *433*, 701–705.

Wiegelmann, T., B. Inhester, B. Kliem, G. Valori, and T. Neukirch (2006a), Testing non-linear force-free coronal magnetic field extrapolations with the Titov-Démoulin equilibrium, *Astron. Astrophys.*, *453*, 737–741, doi:10.1051/0004-6361:20054751.

Wiegelmann, T., B. Inhester, and T. Sakurai (2006b), Preprocessing of vector magnetograph data for a nonlinear force-free magnetic field reconstruction, *Sol. Phys.*, *233*, 215–232.

Wu, S. T., H. M. Chang, and M. J. Hagyard (1985), On the numerical computation of nonlinear force-free magnetic fields, in *Measurements of Solar Vector Magnetic Fields*, NASA Conf. Publ., *2374*, 17–40.

Wu, S. T., M. T. Sun, H. M. Chang, M. J. Hagyard, and G. A. Gary (1990a), On the numerical computation of nonlinear force-free magnetic fields, *Astrophys. J.*, *362*, 698–708.

Wu, S. T., M. T. Sun, and T. Sakurai (1990b), A comparison between progressive extension method (PEM) and iterative method (IM) for magnetic field extrapolations in the solar atmosphere, *Mem. Soc. Astron. Ital.*, *61*, 477–484.

Yan, Y., and Z. Li (2006), Direct boundary integral formulation for solar non-constant-α force-free magnetic fields, *Astrophys. J.*, *638*, 1162–1168, doi:10.1086/499064.

Yan, Y., and T. Sakurai (2000), New boundary integral equation representation for finite energy force-free magnetic fields in open space above the Sun, *Sol. Phys.*, *195*, 89–109.

Yan, Y., M. J. Aschwanden, S. Wang, and Y. Deng (2001a), Evolution of magnetic flux rope in the active region NOAA 9077 on 14 July 2000, *Sol. Phys.*, *204*, 27–40, doi:10.1023/A:1014265123601.

Yan, Y., Y. Deng, M. Karlický, Q. Fu, S. Wang, and Y. Liu (2001b), The magnetic rope structure and associated energetic processes in the 2000 July 14 solar flare, *Astrophys. J. Lett.*, *551*, L115–L119, doi:10.1086/319829.

Yang, W. H., P. A. Sturrock, and S. K. Antiochos (1986), Force-free magnetic fields: The magneto-frictional method, *Astrophys. J.*, *309*, 383–391, doi:10.1086/164610.

Yee, K. S. (1966), Numerical solition of initial boundary value problems involving Maxwell's equations in isotropic media, *IEEE Trans. Antennas Propag.*, *AP-14*(4), 302–307.

―――――――――――

T. Wiegelmann, Max-Planck-Institut für Sonnensystemforschung, Max-Planck-Strasse 2, D-37191 Katlenburg-Lindau, Germany. (wiegelmann@mps.mpg.de)